





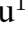






Original Research

Targeting the *AURKB-MAD2L2* Axis Disrupts the DNA Damage Response and Glycolysis to Inhibit Colorectal Cancer Progression

Shengjie Li¹, Jiayou Ye¹, Kaifeng Yang¹, Chengfan Xu¹, Zhixiang Qin¹,
Yiyang Xue², Lanjian Yu¹, Tianyu Zhou¹, Ziming Yin³, Bin Sun^{4,*}, Jun Xu^{1,*}

¹Department of Gastroenterology Surgery, Yichang Central People's Hospital, The First College of Clinical Medical Science, China Three Gorges University, 443000 Yichang, Hubei, China

²Department of Chemistry and Biochemistry, University of California, Santa Barbara, CA 93106, USA

³Department of Chemistry, University of Warwick Coventry, CV4 7AL Coventry, UK

⁴Center for Clinical Research and Translational Medicine, Yangpu Hospital, School of Medicine, Tongji University, 200438 Shanghai, China

*Correspondence: binsun@tongji.edu.cn (Bin Sun); 26720772@qq.com (Jun Xu)

Academic Editor: Graham Pawelec

Submitted: 31 September 2024 Revised: 14 November 2024 Accepted: 31 December 2024 Published: 17 February 2025

Abstract

Background: Dysregulated metabolic pathways, including glycolysis and a compromised DNA damage response (DDR), are linked to the progression of colorectal cancer (CRC). The mitotic arrest deficient-like 2 (*MAD2L2*) and aurora kinase B (*AURKB*) genes play roles in cell cycle regulation and the DDR, making them potential targets for CRC therapy. **Methods:** Differential expression analysis was performed using The Cancer Genome Atlas-Colon Adenocarcinoma (TCGA-COAD) and GSE47074 datasets. A predictive model was established, and gene expression levels were further analyzed. The Gene Expression Profiling Interaction Analysis database and co-immunoprecipitation experiments assessed the correlation between *AURKB* and *MAD2L2*. Knockdown experiments in CRC cell lines further investigated the role of *AURKB*, followed by analyses of cell behavior, oxidative stress, glycolysis, DDR, and interaction with *MAD2L2*. **Results:** The risk model identified six prognostic genes (*BUB1* mitotic checkpoint serine/threonine kinase B (*BUB1B*), *AURKB*, aurora kinase A (*AURKA*), exonuclease 1 (*EXO1*), topoisomerase II alpha (*TOP2A*), cyclin A2 (*CCNA2*)) associated with CRC, which were significantly expressed in tumor samples from the TCGA-COAD and GSE47074 datasets. *In vitro* assays confirmed that *AURKB* knockdown inhibited CRC cell behavior, induced G1 cell cycle arrest, and increased oxidative stress and apoptosis. *AURKB* knockdown also impaired glycolysis, reducing lactate production, glucose uptake, and ATP levels. Overexpression of *MAD2L2* partially reversed these effects, restored glycolytic activity, and mitigated the cell cycle arrest and DDR caused by *AURKB* knockdown. **Conclusion:** *AURKB* regulates CRC progression by modulating glycolysis and DDR pathways. Targeting the *AURKB-MAD2L2* axis offers a promising therapeutic strategy for disrupting fundamental metabolic and DNA repair mechanisms in CRC.

Keywords: colorectal cancer; *AURKB*; *MAD2L2*; DNA damage response; glycolysis

1. Introduction

Colorectal cancer (CRC) is considered one of the most prevalent and lethal cancers globally, imposing a substantial health burden due to its high incidence and mortality [1]. According to global cancer statistics, approximately 1.9 million new cases of CRC are diagnosed each year, accounting for about 10% of all new cancer cases. About 935,000 people die of CRC each year, accounting for 9.2% of all cancer deaths [2]. The incidence of CRC significantly increases with age, especially in individuals over 50 years of age. However, in recent years, the incidence of this disease has also gradually increased in people younger than 50. Globally, the incidence of CRC is slightly higher in men than in women. The incidence of CRC is higher in North America, Europe, Australia, and New Zealand, whereas in some parts of Asia and Africa, the incidence is relatively low. However, it is worth noting that the incidence of CRC is increasing in East Asia. Risk factors for CRC include a family history of bowel cancer, unhealthy eating habits

(e.g., high-fat, low-fiber diets), physical inactivity, smoking, and alcohol consumption [3]. Despite advancements in treatment approaches such as radiotherapy, chemotherapy, and surgical resection, the prognosis for advanced-stage CRC remains poor, highlighting the urgent need for more effective therapeutic strategies [4]. Recent research has increasingly recognized the role of metabolic reprogramming, particularly aerobic glycolysis, in cancer progression [5]. In several malignancies, such as breast and lung cancers, enhanced glycolysis is closely associated with aggressive tumor behavior and poor clinical outcomes. For example, in breast cancer, heightened glycolysis is correlated with increased tumor invasiveness [6], whereas in lung cancer, the overexpression of key glycolytic enzymes such as hexokinase 2 (HK2) drives tumor growth and metastasis [7]. The above findings highlight the critical necessity of targeting aerobic glycolysis during cancer treatment.

The serine/threonine kinase aurora kinase B (*AURKB*) is essential for chromosome segregation and cytokinesis,



making it a significant focus in cancer research [8]. Abnormal *AURKB* activity during cell division can lead to chromosomal instability and uncontrolled cell proliferation [9], both of which are critical drivers of tumorigenesis. Research on CRC has revealed that inhibiting *AURKB* could elevate the susceptibility of CRC cells to fluorouracil, delay the development of chemoresistance, and improve chemotherapy outcomes [10]. Furthermore, in other malignancies such as thyroid cancer, *AURKB* has been tied to cancer development and inhibition of apoptosis [11], underscoring its significance in aggressive tumor behavior.

Mitotic arrest deficient-like 2 (*MAD2L2*) is another key regulator involved in mitotic checkpoint control and the DNA damage response (DDR) [12]. Its involvement in cancer has been extensively documented, particularly for its contribution to tumorigenesis and treatment resistance [13]. In ovarian cancer, high levels of *MAD2L2* correlate with a poor prognosis, partly due to its role in repairing DNA double-strand breaks (DSBs) via the non-homologous end-joining pathway [14]. Similarly, in glioblastoma, *MAD2L2* overexpression promotes tumor progression by enhancing cell survival and proliferation [13]. Emerging evidence suggests a functional connection between *MAD2L2* and *AURKB*. In bladder cancer, *AURKB* has been shown to activate *MAD2L2* expression while downregulating the p53 DDR pathway, which promotes cancer development [15]. Moreover, recent study indicates that *MAD2L2* may influence aerobic glycolysis by regulating vital glycolytic enzymes, contributing to the metabolic reprogramming essential for cancer progression [16].

The DDR is essential for maintaining genomic integrity by detecting and repairing DNA damage [17]. In CRC, dysregulation of the DDR pathway contributes to genomic instability and tumor progression [18]. Alterations in homologous recombination repair (HRR) are increasingly recognized as potential therapeutic targets in CRC [18]. For example, DSBs are crucial for inducing cell death during radiotherapy [19]. However, CRC stem cells can enhance radio resistance by activating cell cycle checkpoints and DDR pathways, facilitating efficient DNA repair and promoting tumor cell survival [20]. This enhanced repair capacity complicates treatment and underscores the potential of targeting DDR mechanisms. The development of DDR-targeted therapies, such as poly (Adenosine diphosphate (ADP)-ribose) polymerase inhibitors, shows promise, especially in treating cancers with HRR deficiencies [21]. Given the complexity and heterogeneity of CRC, understanding the interplay among *AURKB*, *MAD2L2*, and the DDR can unveil new therapeutic strategies and provide valuable insights into CRC treatment and prognosis.

Despite advances in CRC research, the exact mechanisms of CRC development have not been fully elucidated. The goal of this study was to clarify the roles of *AURKB* and *MAD2L2* in CRC progression, focusing on their contributions to glycolysis and DDR. Given the importance of

these pathways in tumor growth and survival, understanding the connection between *AURKB* and *MAD2L2* may reveal novel therapeutic strategies.

2. Material and Methods

2.1 Identification of Differentially Expressed Genes and Intersection Analysis

The Gene Expression Omnibus database (<https://www.ncbi.nlm.nih.gov/gds/?term=GSE47074>) provided the GSE47074 dataset, which included four primary colon cancer samples (tumor group) and four standard samples (control group). In addition, The Cancer Genome Atlas (TCGA) (<https://tcga-data.nci.nih.gov/tcga/>) database provided 414 colon adenocarcinoma (COAD) samples (tumor group) and 41 standard samples (control group). Differentially expressed genes (DEGs) in the two datasets were obtained separately utilizing the limma package in R studio (version 4.0, <http://www.bioconductor.org/packages/release/bioc/html/limma.html>). Genes with fold change (FC) >2 were classified as upregulated, whereas genes with FC <0.5 were considered downregulated, with significance established at $p < 0.05$. The ggplot2 package (<https://cran.r-project.org/package=ggplot2>) in R was utilized to visualize the DEGs. Then the up- and downregulated DEGs in TCGA-COAD and GSE47074 were cross-analyzed using the Bioinformatics and Evolutionary Genomics (<http://bioinformatics.psb.ugent.be/webtools/Venn/>) tool to obtain the genes in the intersection.

2.2 Protein–Protein Interaction Network and Intersection Gene Identification

Next, protein–protein interaction (PPI) network analysis was conducted on overlapping genes utilizing the Search Tool for the Retrieval of Interacting Genes (STRING) (<http://string-db.org/>) database. Subsequently, the Cytohubba plugin in Cytoscape (version 3.8.2, IBM, Armonk, NY, USA) was used to apply the maximum clique centrality (MCC), maximum neighborhood component (MNC), and degree algorithms to identify the top 20 genes of three key modules. Lastly, we performed intersection analysis of the genes from these three network modules to pinpoint the essential intersection genes critical for further investigation.

2.3 Establishment of a Risk Model and Identification of Prognosis-Related Hub Genes

To investigate the 15 essential intersection genes in the TCGA-COAD dataset, we implemented the least absolute shrinkage and selection operator (LASSO) Cox regression algorithm using the glmnet package in R (version 4.0, <http://cran.r-project.org/web/packages/glmnet/index.html>). A LASSO Cox regression model was built with 10-fold cross-validation, plotting the relationship between the logarithm of lambda (λ) and the partial likelihood deviation. The final coefficients for the characteristic genes were determined, which facilitated samples to be classified as high or low risk

according to the expression of crucial ferroptosis genes in the TCGA-COAD database. Then a risk model was established to analyze the survival status, survival time, and gene cluster distribution of these groups. The survival package in R was utilized to create Kaplan-Meier (KM) survival curves and calculate overall survival (OS) probabilities. The 95% confidence intervals (CIs) and hazard ratios (HRs) were computed using the log-rank test and univariate Cox proportional hazard regression. To evaluate prognostic power, receiver operating characteristic (ROC) curves were constructed for 1-, 3-, and 5-year survival rates, with the area under the curve [22] used to assess diagnostic accuracy. Lastly, prognosis-related gene expression was examined in the tumor and control groups from the TCGA-COAD and GSE47074 datasets using the Sangerbox platform (version 3.0, SangerBox Bioinformatics, Beijing, China; available at <http://vip.sangerbox.com/home.html>), leading to identification of the hub gene in this study.

2.4 Analysis of *AURKB* and *MAD2L2* Expression Correlation

The association of *AURKB* and *MAD2L2* expression levels was investigated utilizing the Gene Expression Profiling Interactive Analysis (GEPIA) database (<http://gepia.cancer-pku.cn/>) to learn more about the link between the two. The correlation coefficient across the two genes was obtained. $p < 0.05$ was considered statistically significant.

2.5 Cell Line Cultivation Procedures

CRC cell lines (LoVo, HCT-116, and SW480) and the NCM460 normal human colon mucosal epithelial cell line were purchased from the American Type Culture Collection (ATCC, Shanghai, China). Cells were cultured in Dulbecco's Modified Eagle Medium supplemented with 10% fetal bovine serum, 100 U/mL penicillin, and streptomycin (all from Sangon, Shanghai, China) at 37 °C in a humidified incubator with 5% CO₂. All cell lines were validated by STR profiling and tested negative for mycoplasma. Detailed validation results are provided in **Supplementary Fig. 1**.

2.6 Transfection Assay

CRC cells were plated in 6-well dishes at a density of 5×10^5 cells per well. Once the cells were 70–80% confluent, they were transfected with 10 µL Lipofectamine™ 2000 (Invitrogen, Shanghai, China) according to the manufacturer's instructions. For *AURKB* knockdown, two distinct small interfering RNAs (siRNAs) targeting *AURKB* were transfected into the cells. Non-targeting negative control small interfering RNA (si-NC) was utilized as a negative control. To overexpress *MAD2L2*, a *MAD2L2* expression vector was used to transfect the cells, with empty vector as the control. Two days after transfection, cells were collected for further analysis. The sequence of *si-AURKB-1* was: 5'-GGAGGAGGAUCUACUGAUGAUU

CUAGA-3' (forward), 5'-UCUAGAAUCAAGUAGAUC CUCCUCC-3' (reverse); the sequence of *si-AURKB-2* was 5'-GAUCAUGGAGGAGGAGUUGGCAGAUGCU-3' (forward), 5'-AGCAUCUGCCAACUCCUCCAUGAUC-3' (reverse).

2.7 Quantitative PCR

Total RNA was extracted from CRC cells using TRIzol reagent (9109, Takara, Dalian, China), and complementary DNA (cDNA) was synthesized using the Prime-Script™ RT Reagent Kit (RR047A, Takara, Dalian, China). SYBR Green (RR820A, Takara, Dalian, China)-based quantitative PCR (qPCR) was conducted on the CFX96 Real-Time PCR Machine (1855195, Bio-Rad, Hercules, CA, USA) according to standard qPCR procedures. The $2^{-\Delta\Delta C_t}$ method was employed to quantify the gene expression levels, with *GAPDH* serving as an internal control. The range of primer sequences utilized in qPCR is summarized in Table 1.

2.8 Western Blot Analysis

Proteins were extracted from cultured cells with Radioimmunoprecipitation Assay (RIPA) buffer (P0013B, Beyotime, Shanghai, China) containing phosphatase and protease inhibitors. Then the cell lysate was centrifuged for 20 min, and proteins were quantified with a bovine serum albumin (BSA) protein assay kit (P0010, Beyotime, Shanghai, China). Equal protein concentrations were resolved by sodium dodecyl sulfate polyacrylamide gel electrophoresis (SDS-PAGE) and electrotransferred to PVDF membranes (Beyotime, Shanghai, China). Then the membranes were incubated overnight at 4 °C with the following primary antibodies (all from Abcam, Shanghai, China): *AURKB* (1:1000, ab2254), cyclin D1 (1:10,000, ab134175), p27 (1:5000, ab32034), p21 (1:1000, ab109520), B-cell lymphoma 2 (Bcl-2; 1:2000, ab182858), Bcl-2-associated X protein (Bax, 1:1000, ab32503), caspase-3 (1:5000, ab32351), pyruvate kinase M2 (PKM2; 1:10,000, 15822-1-AP), lactate dehydrogenase A (LDHA; 1:5000, ab52488), hexokinase 2 (HK2; 1:1000, ab209847), glucose transporter 1 (GLUT1; 1:200, ab150299), *MAD2L2* (1:1000, ab180579), p53 (1:1000, ab32049), H2A histone family member X (H2A.X; 1:5000, ab140498), and *GAPDH* (1:5000, ab8245). After three washes with Tris-Buffered Saline with Tween 20 (TBST), membranes were incubated with horseradish peroxidase conjugated anti-mouse (1:1000, A0216, Beyotime, Shanghai, China) and anti-rabbit (1:1000, A0208, Beyotime, Shanghai, China) antibodies, and placed in an overnight incubation at 4 °C. Proteins were detected using enhanced chemiluminescence (ECL; Beyotime) and quantified with ImageJ software (version 1.8.0, National Institutes of Health, Bethesda, MD, USA).

Table 1. Primer sequences for qPCR.

Target	Direction	Sequence (5'-3')
<i>AURKB</i>	Forward	AGATCGAAATCCAGGCCAC
<i>AURKB</i>	Reverse	CCTCCATGATCGTGGCTGTT
<i>Cyclin D1</i>	Forward	GATGCCAACCTCCTCAACGA
<i>Cyclin D1</i>	Reverse	ACTTCTGTTCTCGCAGACC
<i>p27</i>	Forward	CAGCTTGCCCGAGTTCTACT
<i>p27</i>	Reverse	CGACGGATCAGTCTTTGGGT
<i>p21</i>	Forward	AGTCAGTTCCTTGTGGAGCC
<i>p21</i>	Reverse	CATTAGCGCATCACAGTCGC
<i>Bcl-2</i>	Forward	AAAAATACAACATCACAGAGGAAGT
<i>Bcl-2</i>	Reverse	GACGAGGGGGTGTCTTCAAT
<i>Bax</i>	Forward	TGATGGACGGGTCCGGG
<i>Bax</i>	Reverse	TGAGACACTCGCTCAGCTTC
<i>Caspase-3</i>	Forward	TGTGAGGCGGTTGTAGAAGAGT
<i>Caspase-3</i>	Reverse	CTTTATTAACGAAAACCAGAGCGCC
<i>PKM2</i>	Forward	CGAGCCTCAAGTCACTCCAC
<i>PKM2</i>	Reverse	GACGAGCTGTCTGGGGATTC
<i>LDHA</i>	Forward	CTCTGGCAAAGTGGATATCTTGAC
<i>LDHA</i>	Reverse	CTCCATACAGGCACACTGGA
<i>HK2</i>	Forward	TGTGAATCGGAGAGGTCCCA
<i>HK2</i>	Reverse	TCCGGAGACGTGATTTTGGC
<i>GLUT1</i>	Forward	GAGCAGCTACCCTGGATGTC
<i>GLUT1</i>	Reverse	GAGGTCCAGTTGGAGAAGCC
<i>MAD2L2</i>	Forward	CAAAGGAGGCAGACAAAGGCG
<i>MAD2L2</i>	Reverse	GTAGACCTCGCGCACGTAGA
<i>p53</i>	Forward	TGACACGCTTCCCTGGATTG
<i>p53</i>	Reverse	TCCGGGGACAGCATCAAATC
<i>H2A.X</i>	Forward	GGTGCTTAGCCCAGGACTTT
<i>H2A.X</i>	Reverse	CCCAGCGCAGACCTATGAAT
<i>GAPDH</i>	Forward	CATGTTGCAACCGGAAGGA
<i>GAPDH</i>	Reverse	ATCACCCGGAGGAGAAATCG

qPCR, quantitative PCR; AURKB, aurora kinase B; Bcl-2, B-cell lymphoma 2; Bax, Bcl-2-associated X protein; PKM2, pyruvate kinase M2; LDHA, lactate dehydrogenase A; HK2, hexokinase 2; GLUT1, glucose transporter 1; MAD2L2, mitotic arrest deficient-like 2; H2A.X, histone family member X; GAPDH, Glyceraldehyde 3-phosphate dehydrogenase.

2.9 Co-Immunoprecipitation

After centrifugation of HCT-116 and LoVo cells, 500 µg protein from each sample was incubated overnight at 4 °C with 2 µg of either anti-AURKB (1:30; ab45145, Abcam), anti-MAD2L2 (1:40; ab180579, Abcam), or IgG control (1:200; ab200699, Abcam). Then the samples were incubated for 2 h with Protein A/G agarose beads (Santa Cruz Biotechnology, Dallas, TX, USA). Boiling in SDS-PAGE loading buffer allowed bound proteins to be eluted from the beads after they had been cleaned with RIPA buffer (P0013B, Beyotime, Shanghai, China). Following SDS-PAGE and electrophoresis to PVDF membranes, the proteins were detected by Western blotting using anti-AURKB and anti-MAD2L2 antibodies. Protein detection was performed using an ECL detection system (P0018S, Beyotime, Shanghai, China).

2.10 Cell Counting Kit-8 Cell Viability Assay

To measure cell viability, CRC cells were trypsinized and plated in 96-well plates at a density of 2×10^3 cells per well. After 0, 1, 2, 3, and 4 days of culture, 10 µL/well of Cell Counting Kit-8 (CCK-8) reagent was added to the cells and incubated for 1 h. The absorbance at 450 nm was determined with a microplate reader (Model 680, Bio-Rad, Hercules, CA, USA).

2.11 Transwell Assay

A Transwell assay was conducted to measure the invasive capabilities of CRC cells. The cells were seeded in the upper chamber of Transwell (Corning, Shanghai, China) that were pre-coated with 80 µL Matrigel (BD Biosciences, Shanghai, China). Then 600 µL complete medium was added to the lower chamber, and 200 µL serum-free media

containing 1×10^4 CRC cells was added to the upper chamber. Utilizing a cotton swab, non-invasive cells on the upper membrane surface were removed during a 48 h incubation at 37 °C. After fixing in 4% paraformaldehyde, cells were stained for 15 min with DAPI (C1002, Beyotime, Shanghai, China). Cells were observed and recorded with an optical microscope (BX53, Olympus, Tokyo, Japan). The same procedure used for the invasion test was applied to the CRC cells plated to the upper chamber, which was not coated with Matrigel for the migration experiment.

2.12 Cell Cycle Assay

Flow cytometry was employed to evaluate cell cycle distribution. After washing cells with cold phosphate-buffered saline (PBS), CRC cells were fixed in 70% ethanol overnight at 4 °C. Then the cells were washed, stained with propidium iodide (PI) solution, and incubated for 30 min at room temperature in the dark. The FACSCalibur™ flow cytometer (342973, BD Biosciences, San Jose, CA, USA) was utilized for flow cytometry, and data were evaluated with FlowJo software (version 10.0, BD Biosciences, San Jose, CA, USA) to quantify the cell cycle phases (G1, S, G2).

2.13 CRC Apoptosis Assay

Apoptosis was assessed using an Annexin V-FITC/PI staining kit (556547, BD Biosciences, San Jose, CA, USA). After washing with cold PBS, CRC cells (1×10^6 cells/mL) were resuspended in Annexin V binding buffer. Utilizing the FACSCalibur™ flow cytometer, cells were stained with 5 µL Annexin V-FITC (556420, BD Biosciences, San Jose, CA, USA) and 5 µL PI, and then incubated in the dark at room temperature for 15 min. Apoptotic cells were quantified as Annexin V-positive/PI-negative (early apoptosis) and Annexin V-positive/PI-positive (late apoptosis) using FlowJo software (version 10.0, BD Biosciences, San Jose, CA, USA).

2.14 Detection of Malondialdehyde, LDH, and Superoxide Dismutase

To measure the levels of malondialdehyde (MDA) (cat.no. S0131S), LDH (cat.no. C0016), and superoxide dismutase (SOD) (cat. no. S0101S), detection assay kits were used (Beyotime, Shanghai, China). Briefly, CRC cells (5×10^3 cells/well) were seeded in 96-well plates and allowed to adhere. Then reaction mixtures for LDH, MDA, and SOD detection were added to the wells and incubated for 30 min according to the manufacturer's instructions. Finally, the cells were gently washed with PBS, and the respective detection kits were used to quantify the levels of LDH, superoxide dismutase (SOD), and malondialdehyde (MDA).

2.15 Detection of Reactive Oxygen Species

The levels of intracellular reactive oxygen species (ROS) of CRC cells were measured using a ROS detection kit (E004-1-1, Nanjing Jiancheng Bioengineering Institute, Nanjing, China). Briefly, HCT-116 and LoVo cells were plated at a density of 2×10^4 cells/well in 96-well plates. Then the CRC cells were incubated for 30 min in the dark with 10 µM 2',7'-dichlorofluorescein diacetate (DCFH-DA, P0011, Beyotime Biotechnology, Shanghai, China). After incubation, the cells were rinsed three times in serum-free medium, and ROS levels were quantified with a microplate reader.

2.16 Detection of Lactic Acid and Glucose

Lactate levels and glucose uptake levels in CRC cells were assessed using lactate (cat.no. A019-2-1) and glucose assay kits (cat.no. F006-1-1), respectively, according to the manufacturer's instructions (Nanjing Jiancheng Bioengineering Institute, Nanjing, China). Briefly, 200 µL culture medium per well of 96-well plates were used to seed 2×10^4 cells. Following 48 h of culture, the supernatant culture medium was collected, and lactate and glucose levels were assessed using a colorimetric assay according to the manufacturer's instructions. Lactate production rates and glucose consumption were normalized to cell count to ensure accurate sample comparisons.

2.17 Detection of ATP Levels

Intracellular ATP levels were measured using an ATP assay kit (S0026, Beyotime, Shanghai, China). Briefly, after collecting the cells, they were lysed with 200 µL lysis buffer and centrifuged at 12,000 rpm at 4 °C; the supernatant was removed as the test sample. Subsequently, 100 µL ATP detection reagent and 10 µL test sample were mixed following the manufacturer's instructions, and the luminescence was measured using a NanoDrop spectrophotometer (ND-2000, Thermo Fisher Scientific, Waltham, MA, USA). A standard curve was used to calculate the relative ATP levels, which then were normalized to cell number or protein concentration to ensure accurate comparisons.

2.18 Statistical Analyses

R was used as the programming language for data analyses. Two groups were compared using the unpaired Student's *t*-test. One-way analysis of variance and Tukey's post hoc test were used for multiple group comparisons. $p < 0.05$ was considered statistically significant. Each experiment, unless otherwise noted, was carried out in triplicate.

3. Results

3.1 Differential Expression and PPI Network Analysis to Identify Essential CRC Genes

Initially, we conducted differential expression analysis on the GSE47074 and TCGA-COAD datasets. Fig. 1A

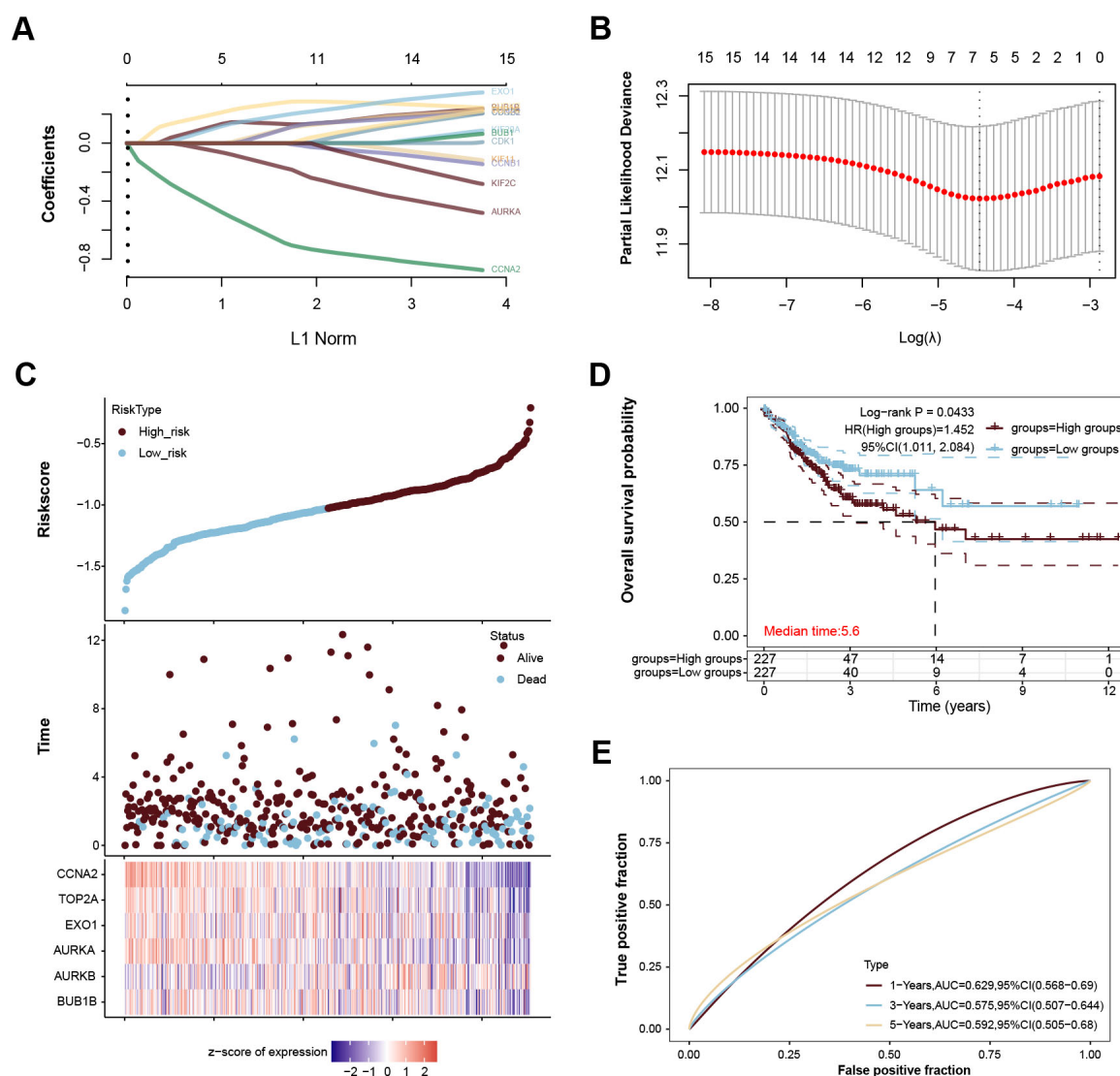


Fig. 2. Construct a prognostic-related risk model through LASSO regression analysis. (A) Processes of LASSO Cox model fitting. Each curve represents a CRC-related gene. (B) Selection of the optimal λ value in the LASSO model using 10-fold cross-validation. The red dots represent the partial likelihood of deviance for each value of λ , with the vertical dotted line indicating the optimal λ corresponding to the minimum deviance. (C) Distribution of risk scores in the high- and low-risk groups. The top panel displays the risk scores, the middle panel indicates the survival status (alive or dead), and the bottom panel shows a heatmap of the z-scores of gene expression levels for the six selected genes. (D) KM survival curves comparing OS between the high- and low-risk groups. Patients in the high-risk group had significantly worse OS (log-rank $p = 0.0433$, HR = 1.452, 95% CI: 1.011, 2.084). The median survival time for the high-risk group was 5.6 years. (E) Time-dependent ROC curves for the predictive model, showing AUC values of 0.629, 0.575, and 0.592 for 1-, 3-, and 5-year survival predictions, respectively. CRC, colorectal cancer; LASSO, least absolute shrinkage and selection operator; COAD, colon adenocarcinoma; KM, Kaplan-Meier; OS, overall survival; HR, hazard ratio; CI, confidence interval; ROC, receiver operator characteristic; AUC, area under the curve; CCNA2, cyclin A2; TOP2A, DNA topoisomerase II alpha; EXO1, exonuclease 1; BUB1B, BUB1 mitotic checkpoint serine/threonine kinase B.

3.2 Construction of Risk Model and Identification of Genes Associated with CRC Prognosis

We performed LASSO Cox regression analysis for 15 intersecting genes to identify the critical genes connected with COAD prognosis. The LASSO coefficient spectrum of the candidate genes is shown in Fig. 2A. The optimal value of the regularization parameter (λ) was ob-

tained via 10-fold cross-validation based on the minimum partial likelihood deviation (Fig. 2B). Six genes (cyclin A2 [CCNA2], DNA topoisomerase II alpha [TOP2A], exonuclease 1 [EXO1], AURKA, AURKB, and BUB1 mitotic checkpoint serine/threonine kinase B [BUB1B]) were selected to construct the predictive risk model. Next, each patient's risk score was determined by calculating the ex-

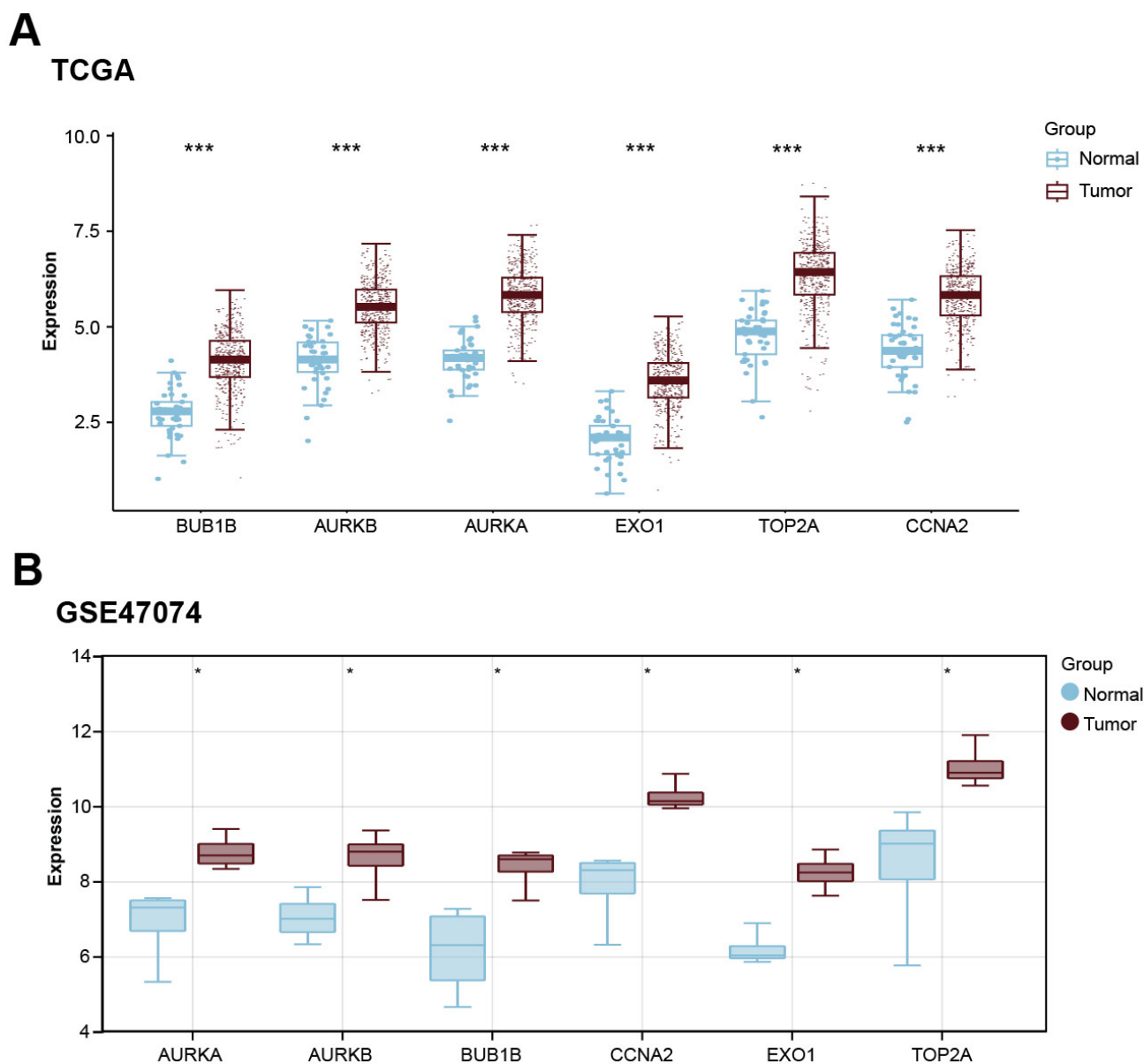


Fig. 3. Expression of six prognosis-related genes. (A) Box plot of the expression levels of six prognostic genes (*BUB1B*, *AURKB*, *AURKA*, *EXO1*, *TOP2A*, and *CCNA2*) in COAD versus normal tissues in TCGA-COAD dataset. (B) Box plot of the expression levels of six prognostic genes (*BUB1B*, *AURKB*, *AURKA*, *EXO1*, *TOP2A*, and *CCNA2*) in normal and tumor samples in the GSE47074 dataset. * $p < 0.05$, *** $p < 0.001$. TCGA-COAD, The Cancer Genome Atlas-Colon Adenocarcinoma.

pression of these six genes. The median risk score divided patients into high- and low-risk categories. The risk scores, clinical survival time, and gene expression z -scores of all samples were visualized, and the findings revealed that the clinical survival time of high-risk patients was considerably worse (Fig. 2C). KM survival analysis showed that individuals at high risk had a substantially lower overall survival (OS) than those at low risk (log-rank $p = 0.0433$, HR = 1.452, 95% CI: 1.011, 2.084; Fig. 2D). In addition, the ROC curve was used to evaluate the predictive performance of the risk model, with 1-, 3-, and 5- survival rates yielding area under the curve (AUC) values of 0.629, 0.575, and 0.592, respectively (Fig. 2E).

3.3 Prognosis-Related Gene Expression Analysis

TCGA-COAD and GSE47074 datasets were used to examine the expression of these six genes (*BUB1B*, *AURKB*, *AURKA*, *EXO1*, *TOP2A*, and *CCNA2*), and it was discovered that all of the genes had greater expression levels in the tumor groups of both datasets (Fig. 3A,B). Among these, *AURKB* was an interesting gene due to its function in controlling mitosis, a critical stage of the cell cycle. Disruption of mitosis by DNA damage can severely impair cell division, and aerobic glycolysis is known to supply the energy necessary for the DDR [23]. Given its potential involvement in the aerobic glycolysis of CRC cells, *AURKB*

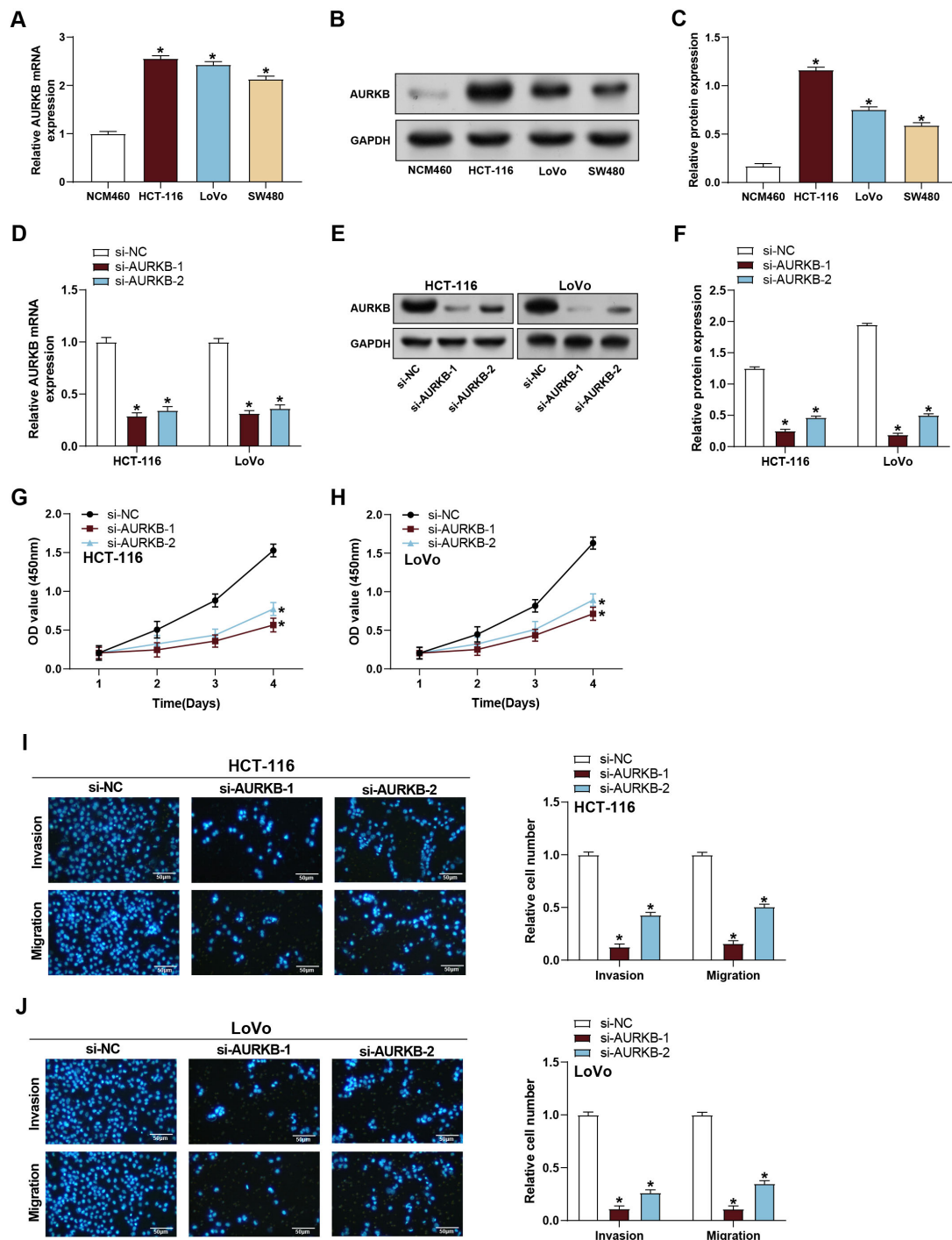


Fig. 4. Knockdown of *AURKB* inhibits CRC cell proliferation, invasion, and migration. (A) The qPCR data of *AURKB* mRNA expression in NCM450, HCT-116, LoVo, and SW480 cells. (B,C) Western blot analysis of *AURKB* protein expression levels in NCM450, HCT-116, LoVo, and SW480 cells. (D) qPCR data of *AURKB* mRNA expression in HCT-116 and LoVo cells after *AURKB* knockdown. (E,F) Western blot analysis of *AURKB* protein expression levels in HCT-116 and LoVo cells after *AURKB* knockdown. (G,H) CCK-8 assay detected the proliferation of HCT-116 (G) and LoVo (H) cells on days 0–4 after knockdown of *AURKB*. The X-axis is time (days), and the Y-axis is the optical density value when the absorbance was 450 nm. (I,J) Transwell assay detected the invasion and migration abilities of HCT-116 (I) and LoVo. Scale bar: 50 μ m. (J) Cells after *AURKB* knockdown. Scale bar: 50 μ m. * p < 0.05. qPCR, quantitative PCR; CRC, colorectal cancer; CCK-8, cell counting kit-8; *AURKB*, aurora kinase B; si-NC, small interfering RNA negative control.

was determined as the core gene in this investigation, warranting further investigation into its role in CRC progression.

3.4 Knockdown of *AURKB* Inhibits CRC Cell Behaviors

To investigate the function of the hub gene *AURKB* in CRC, qPCR was carried out to assess *AURKB* expression in NCM460 cells and three CRC cell lines. The findings revealed that the *AURKB* mRNA levels in the three CRC cells were significantly higher than those in normal colon epithelial cells, of which the expression of *AURKB* in LoVo and HCT-116 cells was the highest (Fig. 4A). This finding was corroborated by Western blot analysis, as illustrated in Fig. 4B,C. Subsequently, the expression of *AURKB* was knocked down in CRC cells, and the findings demonstrated a significant reduction in expression levels following *AURKB* knockdown compared to the control group (Fig. 4D–F). CCK-8 assays showed that the proliferation of CRC cells was reduced following *AURKB* silencing (Fig. 4G,H). A transwell assay was carried out to assess the invasion and migration of LoVo and HCT-116 cells following *AURKB* knockdown. The results showed that knockdown of *AURKB* significantly inhibited the metastasis of CRC cells (Fig. 4I,J).

3.5 *AURKB* Knockdown Induces CRC Cell Arrest in the G1 Phase

After *AURKB* knockdown, flow cytometry results showed that the proportion of cells in the G1 phase significantly increased, whereas the proportion of cells in the S phase significantly decreased. These results suggest that *AURKB* knockdown blocked cells in the G1 phase by inhibiting the G1/S transition (Fig. 5A,B). The mRNA expression of key cell cycle regulators, including *cyclin D1*, *p27*, and *p21*, were further examined by qPCR. The results showed that *AURKB* knockdown significantly downregulated *cyclin D1* and upregulated *p27* and *p21* expression in CRC cells (Fig. 5C,D). Western blot analysis confirmed these findings at the protein level, showing decreased protein expression of cyclin D1 and increased p27 and p21 expression after *AURKB* knockdown in both cell lines (Fig. 5E–G). These findings indicate that *AURKB* knockdown causes G1 arrest in CRC cells, possibly through downregulating *cyclin D1* and upregulating cell cycle inhibitors *p27* and *p21*.

3.6 Knockdown of *AURKB* Induces Apoptosis of CRC Cells In Vitro

The effect of *AURKB* knockdown on apoptosis of colon cancer cells was analyzed by flow cytometry, and an apoptosis rate of approximately 8% was observed (Fig. 6A,B). In addition, qPCR and western blotting were conducted to evaluate the expression changes of key apoptotic markers in CRC cells. Consistent with the flow cytometry results, knockdown of *AURKB* enhanced the expres-

sion of caspase-3 and Bax and decreased the expression of Bcl-2 (Fig. 6C–G). We observed significant changes in the expression patterns of apoptosis marker genes. This discrepancy between the relatively low apoptosis rate and the significant changes in expression of apoptosis-associated genes may stem from the complexity of the apoptosis pathway. Apoptosis is a complex process that involves multiple signaling pathways and feedback mechanisms. Knockdown of *AURKB* may have affected multiple apoptosis-associated genes and proteins, but these changes did not all directly lead to cell death. In this process, some genes may play a regulatory role mainly in the apoptotic pathway rather than directly inducing cell death. This complex regulatory network may lead to discrepancies between significant changes in gene expression patterns and the apoptosis rates detected by flow cytometry. Our findings suggest that knockdown of *AURKB* induces apoptosis in CRC cells by regulating the expression of critical apoptotic regulators. Since *si-AURKB-1* showed more pronounced effects in inhibiting cell growth and promoting apoptosis, we selected it for subsequent analyses.

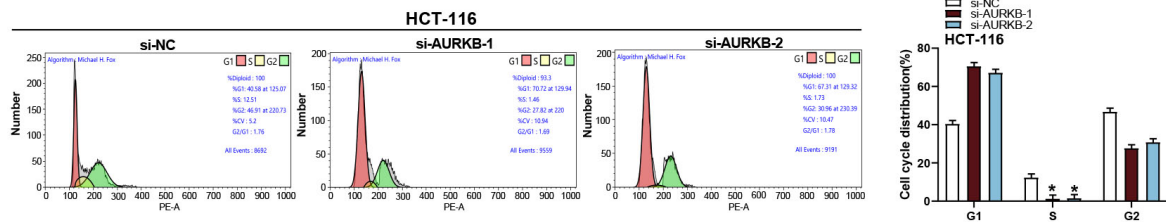
3.7 *AURKB* Knockdown Increases Oxidative Stress and Cell Damage in CRC Cells

To assess the effect of *AURKB* knockdown on oxidative stress in CRC cells, we used detection kits to measure LDH, ROS, MDA, and SOD expression levels in LoVo and HCT-116 cells. As shown in Fig. 7A, knockdown of *AURKB* significantly increased LDH activity in CRC cells, indicating increased cell membrane damage. Similarly, ROS levels were markedly elevated following *AURKB* knockdown in both cell lines (Fig. 7B), suggesting increased oxidative stress. Additionally, MDA levels, a marker of lipid peroxidation, were significantly higher in *AURKB* knockdown cells than controls (Fig. 7C). Conversely, SOD activity, which serves as an antioxidant defense mechanism, was significantly reduced in cells with *AURKB* knockdown (Fig. 7D). These findings indicate that *AURKB* knockdown in CRC cells leads to increased oxidative stress, cellular damage, and lipid peroxidation, which may be involved in the induced apoptosis.

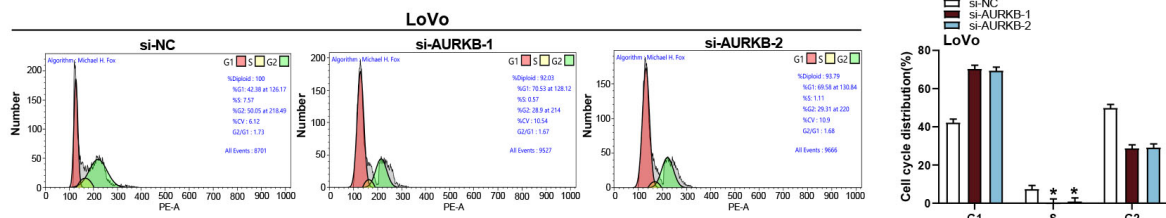
3.8 *AURKB* Knockdown Inhibits Glycolysis and Reduces ATP Generation in CRC Cells

Through kit testing, it was found that *AURKB* knockdown significantly reduced ATP production, glucose uptake, and lactate production in CRC cells compared with the control group (Fig. 8A–C). qPCR was conducted to assess the expression levels of glycolysis-related genes (*PKM2*, *LDHA*, *HK2*, *GLUT1*) in CRC cells. Compared to the control group, the expression of glycolysis-related genes was significantly downregulated after *AURKB* knockdown (Fig. 8D,E). Western blot analysis confirmed that *AURKB* knockdown led to decreased protein expression of *PKM2*, *LDHA*, *HK2*, and *GLUT1* in CRC cells (Fig. 8F–H). These

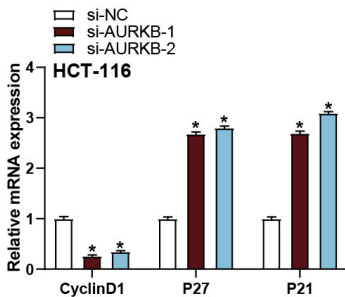
A



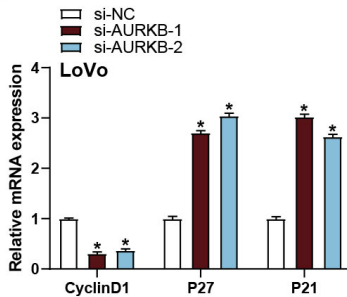
B



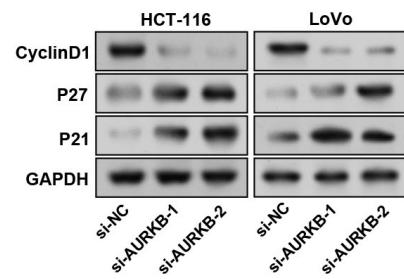
C



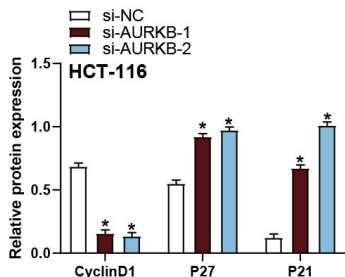
D



E



F



G

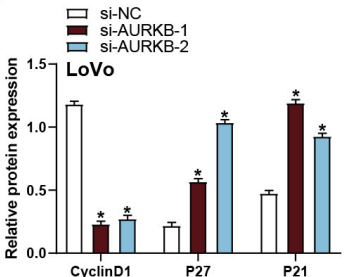


Fig. 5. Effects of *AURKB* knockdown on cell cycle distribution and cell cycle regulators in CRC cells. (A,B) Flow cytometry analysis of cell cycle distribution in HCT-116 (A) and LoVo (B) cells transfected with control siRNA (si-NC) or *AURKB*-specific siRNA (si-AURKB-1 and si-AURKB-2). The bar graph on the right summarizes the percentage of cells in each cell cycle phase (G1, S, G2). (C,D) qPCR analysis of cyclin D1, p27, and p21 mRNA expression levels in HCT-116 (C) and LoVo (D) cells after *AURKB* knockdown. (E–G) Western blot analysis of protein expression of cycle-related proteins cyclin D1, p27, and p21 in HCT-116 and LoVo cells after *AURKB* knockdown. * $p < 0.05$. qPCR, quantitative PCR; CRC, colorectal cancer; siRNA, small interfering RNA; *AURKB*, aurora kinase B; si-NC, small interfering RNA negative control.

results indicate that *AURKB* knockdown impairs glycolysis and energy production in CRC cells by downregulating critical glycolytic enzymes and glucose transporters, thereby decreasing ATP levels.

3.9 *MAD2L2* Overexpression Mitigates the Effects of *AURKB* Knockdown on CRC Cells

The GEPIA database analyzed the expression correlation between *AURKB* and *MAD2L2*. Bioinformatics analysis

revealed a significant positive relationship between the expression levels of *AURKB* and *MAD2L2*, with a correlation coefficient of 0.415 (Fig. 9A). The connection between *AURKB* and *MAD2L2* was further elucidated by co-immunoprecipitation experiments, which further confirmed that *AURKB* can interact with *MAD2L2* in LoVo and HCT-116 cells (Fig. 9B). Subsequently, qPCR was used to detect the significant overexpression efficiency of *MAD2L2* in CRC cells, and Western blotting experimental results also

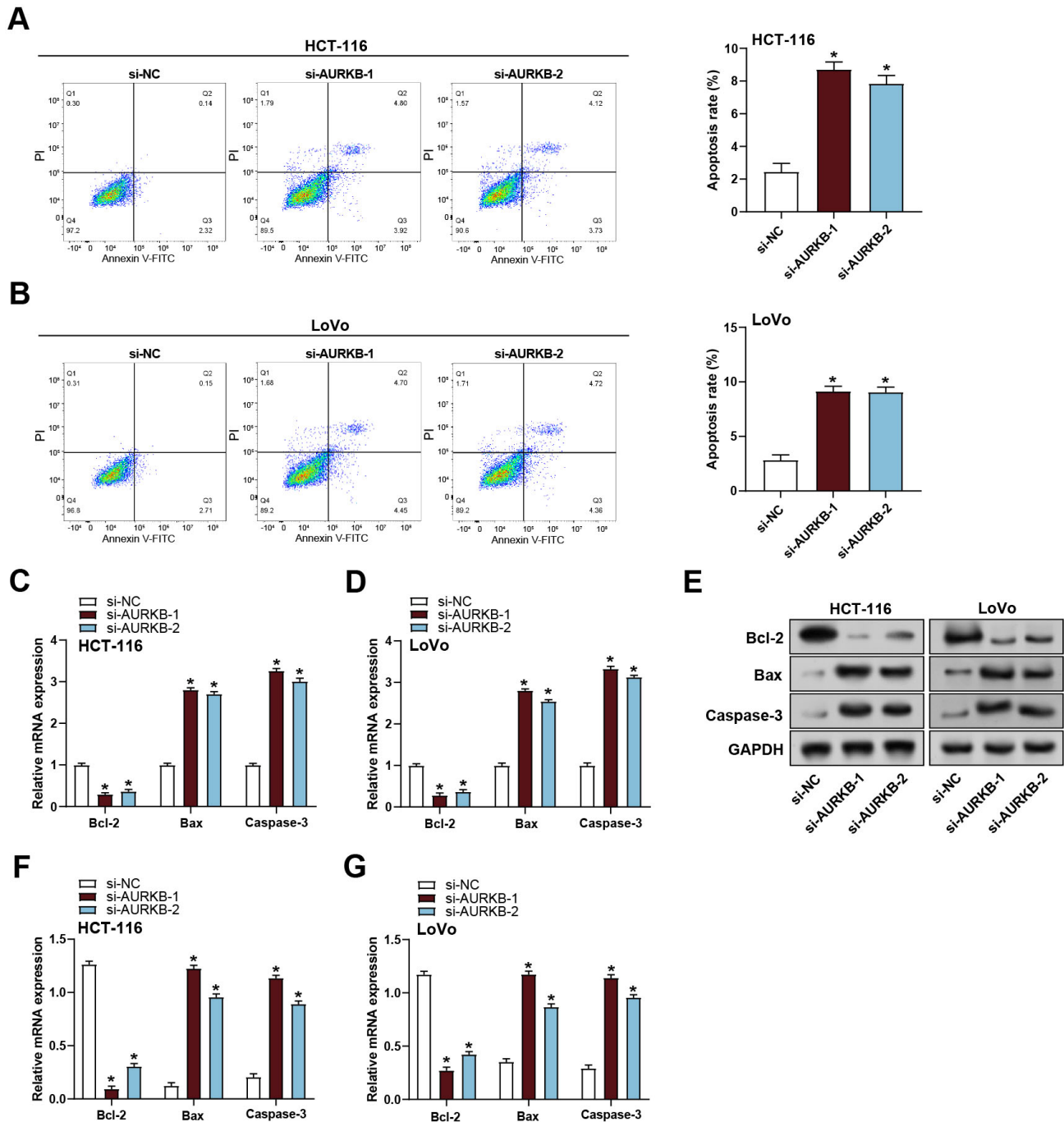


Fig. 6. *AURKB* knockdown induces apoptosis in CRC cells. (A,B) Flow cytometry analysis of apoptosis in HCT-116 (A) and LoVo (B) cells transfected with control siRNA (si-NC) or *AURKB*-specific siRNA (si-*AURKB*-1 and si-*AURKB*-2). The bar graph on the right summarizes the percentage of apoptotic cells in each group. (C,D) qPCR data of mRNA expression of apoptosis-related markers *Bax*, *Bcl*-2, and *caspase*-3 in HCT-116 and LoVo after *AURKB* knockdown. (E–G) Western blot analysis of protein expression of apoptosis-related proteins *Bax*, *Bcl*-2, and *caspase*-3 in HCT-116 and LoVo cells after *AURKB* knockdown. * $p < 0.05$. qPCR, quantitative PCR; CRC, colorectal cancer; *AURKB*, aurora kinase B; siRNA, small interfering RNA; *Bcl*-2, B-cell lymphoma 2; *Bax*, *Bcl*-2-associated X protein.

demonstrated effective knockdown (Fig. 9C–E). The CCK-8 assay demonstrated that *MAD2L2* overexpression significantly reversed the proliferation of CRC cells inhibited by *AURKB* knockdown (Fig. 9F,G). In addition, Transwell ex-

periments performed in CRC cells showed that *MAD2L2* overexpression rescued the inhibitory effects of *AURKB* knockdown on cell behavior (Fig. 9H,I).

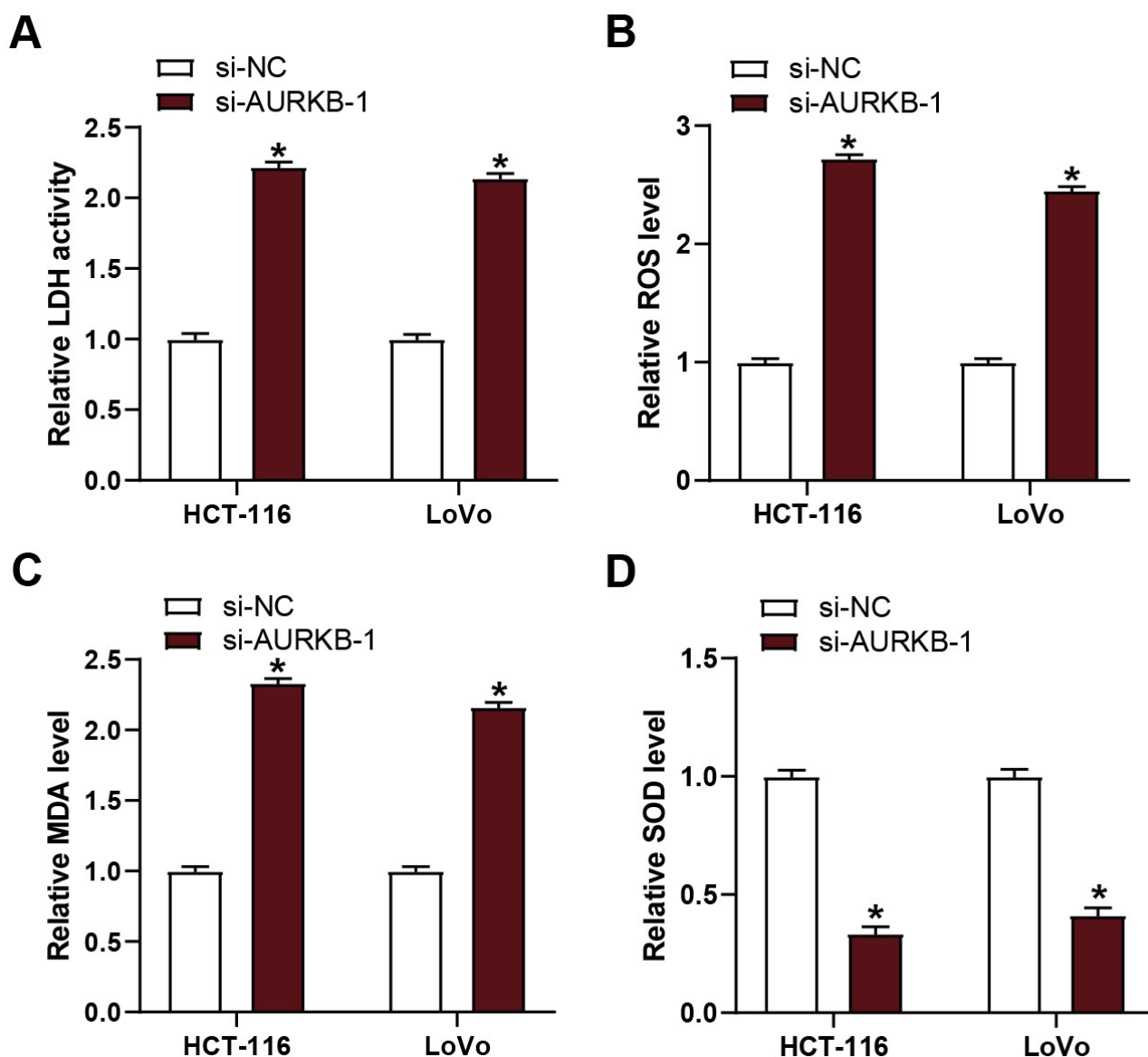


Fig. 7. Knockdown of AURKB affects oxidative stress in CRC cells. (A) Relative LDH activity in HCT-116 and LoVo cells transfected with control siRNA (si-NC) or AURKB-specific siRNA (si-AURKB-1). (B) Relative ROS levels in HCT-116 and LoVo cells following AURKB knockdown. (C) Relative MDA levels in HCT-116 and LoVo cells after AURKB knockdown. (D) Relative SOD levels in HCT-116 and LoVo cells after AURKB knockdown. * $p < 0.05$. CRC, colorectal cancer; LDH, Lactate dehydrogenase; ROS, Reactive oxygen species; MDA, Malondialdehyde; SOD, Superoxide dismutase; AURKB, aurora kinase B; siRNA, small interfering RNA; si-NC, small interfering RNA negative control.

3.10 MAD2L2 Overexpression Alleviates the Effects of AURKB Knockdown on Cell Cycle Inhibition and the p53 DDR Pathway

To understand the impact of *MAD2L2* overexpression on the CRC cell cycle and DDR in the context of *AURKB* knockdown, we evaluated the expression of key cell cycle proteins (cyclin D1, p21, and p53) and DNA damage marker H2A.X in CRC cells. qPCR analysis showed that *AURKB* knockdown significantly reduced *cyclin D1* mRNA expression while increasing *p53*, *p21*, and *H2A.X* expression in CRC cells (Fig. 10A,B). However, overexpression of *MAD2L2* partially reversed these effects, re-

sulting in the restoration of *cyclin D1* levels and decreased expression of *p53*, *p21*, and *H2A.X*. Western blot analysis confirmed these findings at the protein level (Fig. 10C–E). These results suggest that *MAD2L2* overexpression can mitigate the impact of *AURKB* knockdown on DDR and cell cycle progression, highlighting the potential compensatory mechanism in CRC cells. We also observed a decrease in the mRNA and protein expression of *MAD2L2* after knockdown of *AURKB*, suggesting that *AURKB* may have regulatory effects on the expression level of *MAD2L2*. However, we also found that overexpression of *MAD2L2* did not restore the decrease in *AURKB* mRNA and protein ex-

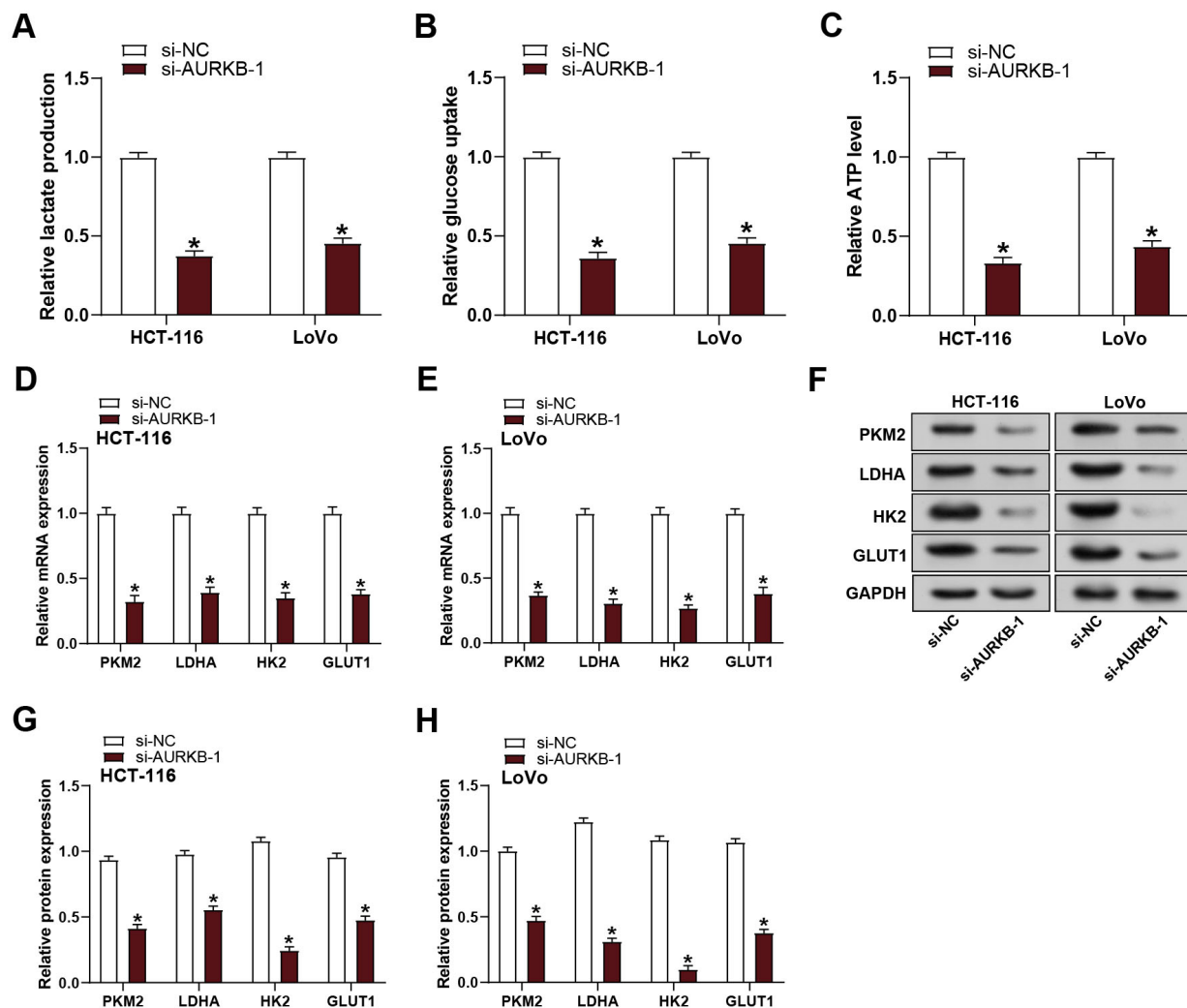


Fig. 8. Effects of *AURKB* knockdown on glycolysis and ATP production in CRC cells. (A) Relative lactate production in HCT-116 and LoVo cells transfected with control siRNA (si-NC) or *AURKB*-specific siRNA (si-*AURKB*-1). (B) Relative glucose uptake in HCT-116 and LoVo cells following *AURKB* knockdown. (C) ATP levels in HCT-116 and LoVo cells after *AURKB* knockdown. (D,E) qPCR data of mRNA expression of glycolysis-related genes *PKM2*, *LDHA*, *HK2*, and *GLUT1* in HCT-116 and LoVo cells after *AURKB* knockdown. (F–H) Western blot analysis of protein expression of glycolysis-related proteins *PKM2*, *LDHA*, *HK2*, and *GLUT1* in HCT-116 and LoVo cells after *AURKB* knockdown. * $p < 0.05$. CRC, Colorectal cancer; qPCR, Quantitative PCR; *AURKB*, Aurora kinase B; siRNA, Small interfering RNA; *PKM2*, Pyruvate kinase M2; *LDHA*, Lactate dehydrogenase; *HK2*, Hexokinase 2; *GLUT1*, Glucose transporter 1.

pression caused by *AURKB* knockdown. This finding suggests that *MAD2L2* may not be directly involved in regulating *AURKB* expression despite the effect of *AURKB* on *MAD2L2* expression.

3.11 *MAD2L2* Overexpression can Reverse the Inhibition of Glycolysis in CRC Cells Caused by *AURKB* Knockdown

Next, ATP levels, glucose uptake, and lactate production in CRC cells were assessed. In contrast to the control, *AURKB* knockdown inhibited ATP levels, lactate production, and glucose uptake, while *MAD2L2* overexpression reversed this inhibitory phenomenon (Fig. 11A–C). The expression of key glycolytic enzymes at the mRNA

and protein levels was further evaluated. qPCR analysis showed that *AURKB* knockdown significantly reduced the mRNA levels of these glycolysis-related genes in CRC cells (Fig. 11D,E). Western blot analysis showed that *PKM2*, *LDHA*, *HK2*, and *GLUT1* protein levels were significantly reduced after *AURKB* knockdown (Fig. 11F). Notably, *MAD2L2* overexpression reversed these effects and restored *PKM2*, *LDHA*, *HK2*, and *GLUT1* levels in *AURKB* knockdown cells (Fig. 11G,H). These results indicate that *MAD2L2* overexpression can restore glycolytic activity and ATP production impaired by *AURKB* knockdown, highlighting its role in maintaining CRC cell metabolism.

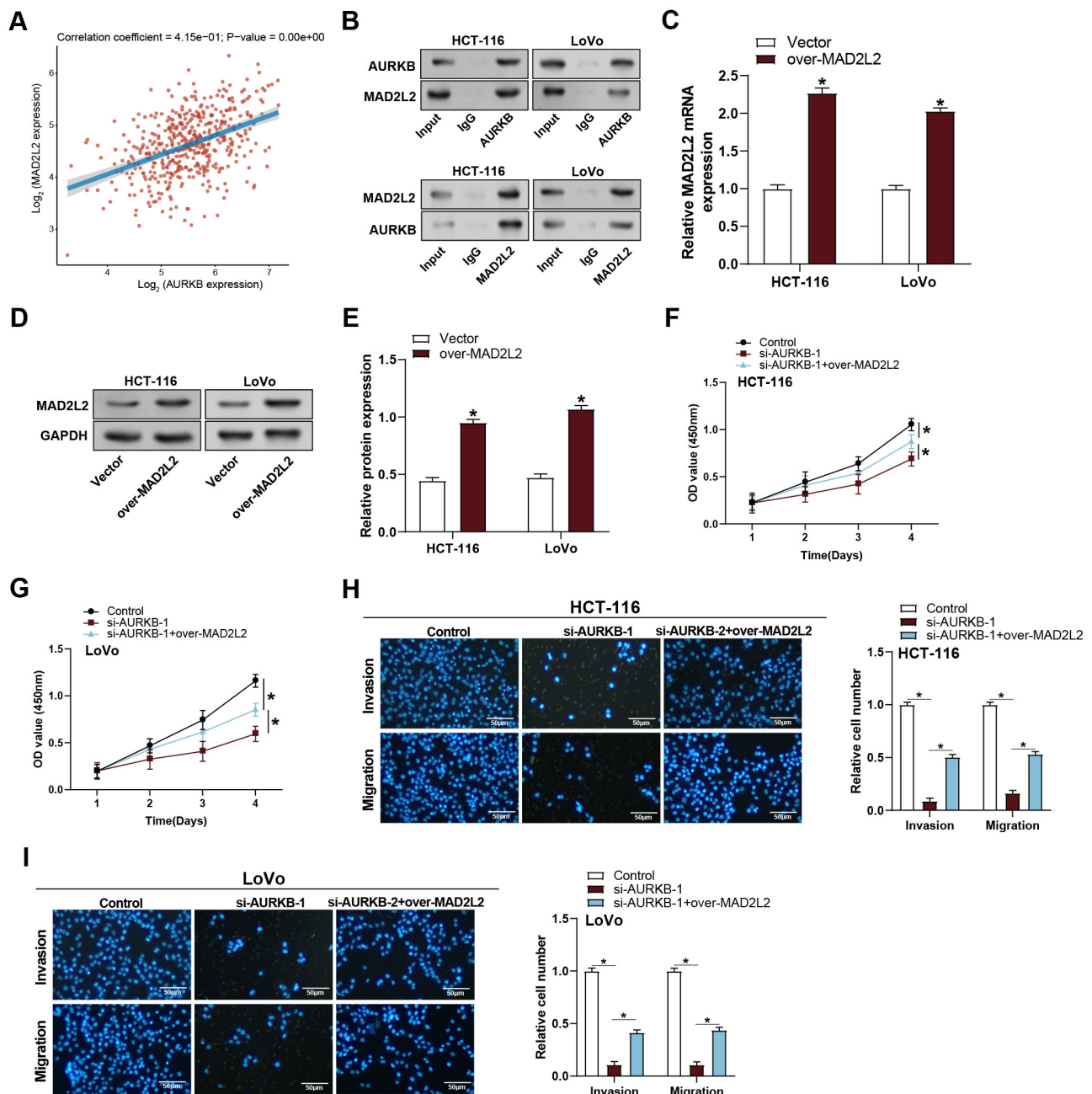


Fig. 9. MAD2L2 overexpression rescues the inhibitory effects of AURKB knockdown on CRC cell proliferation, migration, and invasion. (A) Correlation analysis between AURKB and MAD2L2 expression in CRC detected by the GEPIA database. (B) Co-IP demonstrated the interaction of AURKB and MAD2L2 in HCT-116 and LoVo cells. (C) qPCR data of MAD2L2 mRNA expression in HCT-116 and LoVo after MAD2L2 overexpression. (D,E) Western blot analysis of MAD2L2 protein expression levels in HCT-116 and LoVo cells after MAD2L2 overexpression. (F,G) CCK-8 assay was used to detect the proliferation of control, si-AURKB-1, and si-AURKB-1+over-MAD2L2 treated HCT-116 and LoVo cells from day 0 to day 4. (H,I) Transwell assay detected the invasion and migration abilities of Control, si-AURKB-1, and si-AURKB-1+over-MAD2L2 treated HCT-116 and LoVo cells. Scale bar: 50 μ m. $*p < 0.05$. CRC, colorectal cancer; Co-IP, co-immunoprecipitation; qPCR, quantitative PCR; CCK-8, cell counting kit-8; MAD2L2, mitotic arrest deficient 2 like 2; GEPIA, gene expression profiling interactive analysis.

4. Discussion

CRC is a major worldwide health challenge because of its high morbidity and death rates. Identifying critical genes involved in CRC progression has been a central fo-

cus of recent research. Notable genes such as APC regulator of WNT signaling pathway (*APC*), tumor protein p53 (*TP53*), and KRAS proto-oncogene, GTPase (*KRAS*) have been extensively studied for their roles in CRC. APC muta-

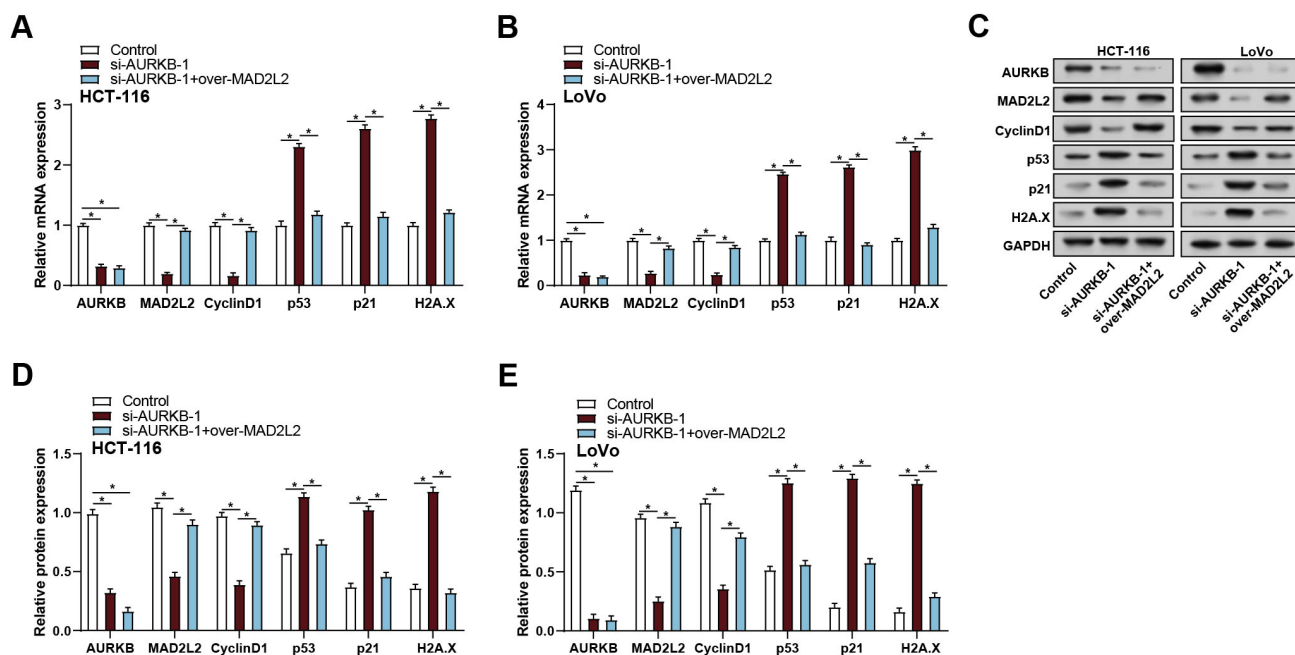


Fig. 10. *MAD2L2* overexpression mitigates the effects of *AURKB* knockdown on cell cycle regulators and the p53 DDR pathway. (A,B) qPCR was used to detect the mRNA expression levels of *AURKB*, *MAD2L2*, *cyclin D1*, *p53*, *p21*, and *H2A.X* in the control group, si-*AURKB*-1, si-*AURKB*-1+over-*MAD2L2* treated HCT-116 and LoVo cells. (C–E) Western blot analysis was used to detect the protein expression levels of *AURKB*, *MAD2L2*, cyclin D1, p53, p21, and H2A.X in the control group, si-*AURKB*-1, si-*AURKB*-1+over-*MAD2L2* treated HCT-116 and LoVo cells. * $p < 0.05$. qPCR, quantitative PCR; DDR, DNA damage response; *AURKB*, aurora kinase B; *MAD2L2*, mitotic arrest deficient 2 like 2; H2A.X, H2A histone family member X.

tions are commonly linked to early-stage CRC [24], while TP53 mutations are associated with advanced disease and poor prognosis [25]. KRAS mutations, on the other hand, are often related to chemotherapy resistance, influencing treatment outcomes [26]. In this research, we obtained six CRC prognosis-related genes through bioinformatics analysis. *AURKA* is linked to a poor prognosis in various cancers and regulates the wntless/integrated (Wnt) and RAS-mitogen-activated protein kinase (Ras-MAPK) signaling pathways, promoting CRC development. *BUB1B*, critical for mitotic checkpoints and genomic stability, is closely linked to CRC development [27]. *CCNA2*, a crucial cell cycle regulator, drives CRC cell proliferation [28]. *EXO1* participates in DNA damage repair and is essential for maintaining genomic stability, with its dysfunction leading to instability [29]. *TOP2A* is crucial for DNA topology regulation and cancer cell proliferation [30]. *AURKB*, essential for cell division and mitosis, was identified as a critical gene in this study, with its role in glycolysis and DDR in CRC cells warranting further investigation.

AURKB is a crucial regulator of mitosis, chromosome segregation, and cytokinesis, with significant implications for cancer cell behavior. Studies have demonstrated that *AURKB* overexpression promotes proliferation and invasion while inhibiting apoptosis in various cancers, including breast cancer and hepatocellular carcinoma [31,32]. In prostate cancer, *AURKB* overexpression is associated with

a poor prognosis and increased tumor aggressiveness [33]. Tumor cell cycle regulation is tightly controlled by proteins such as p27 and p21, which, when downregulated, are linked to accelerated tumor growth and poor outcomes in CRC [34]. Apoptosis-related proteins such as Bcl-2, known for their anti-apoptotic properties, are also upregulated in CRC, contributing to tumor progression [35]. Building upon this knowledge, our study focused on the function of *AURKB* in CRC. We discovered that *AURKB* expression was significantly higher in CRC cells than in normal cells. Knockdown of *AURKB* in CRC cells decreased invasion and proliferation, caused cell cycle arrest, and increased apoptosis. These outcomes offer essential perspectives regarding the molecular processes by which *AURKB* contributes to CRC progression.

Oxidative stress, because it damages cells and tissue and is characterized by an imbalance between the production of ROS and antioxidant defenses, plays an essential role in cancer pathogenesis. Critical factors in this process include LDH, ROS, MDA, and SOD [36]. In CRC, elevated ROS levels inhibit cell growth and migration, and increased MDA levels indicate heightened oxidative damage in CRC tissues compared to normal tissues [37]. Concurrently, aerobic glycolysis, the phenomenon where tumor cells preferentially produce ATP by glycolysis even under aerobic circumstances, is a characteristic of cancer metabolism [38]. Greater lactate generation and better glu-

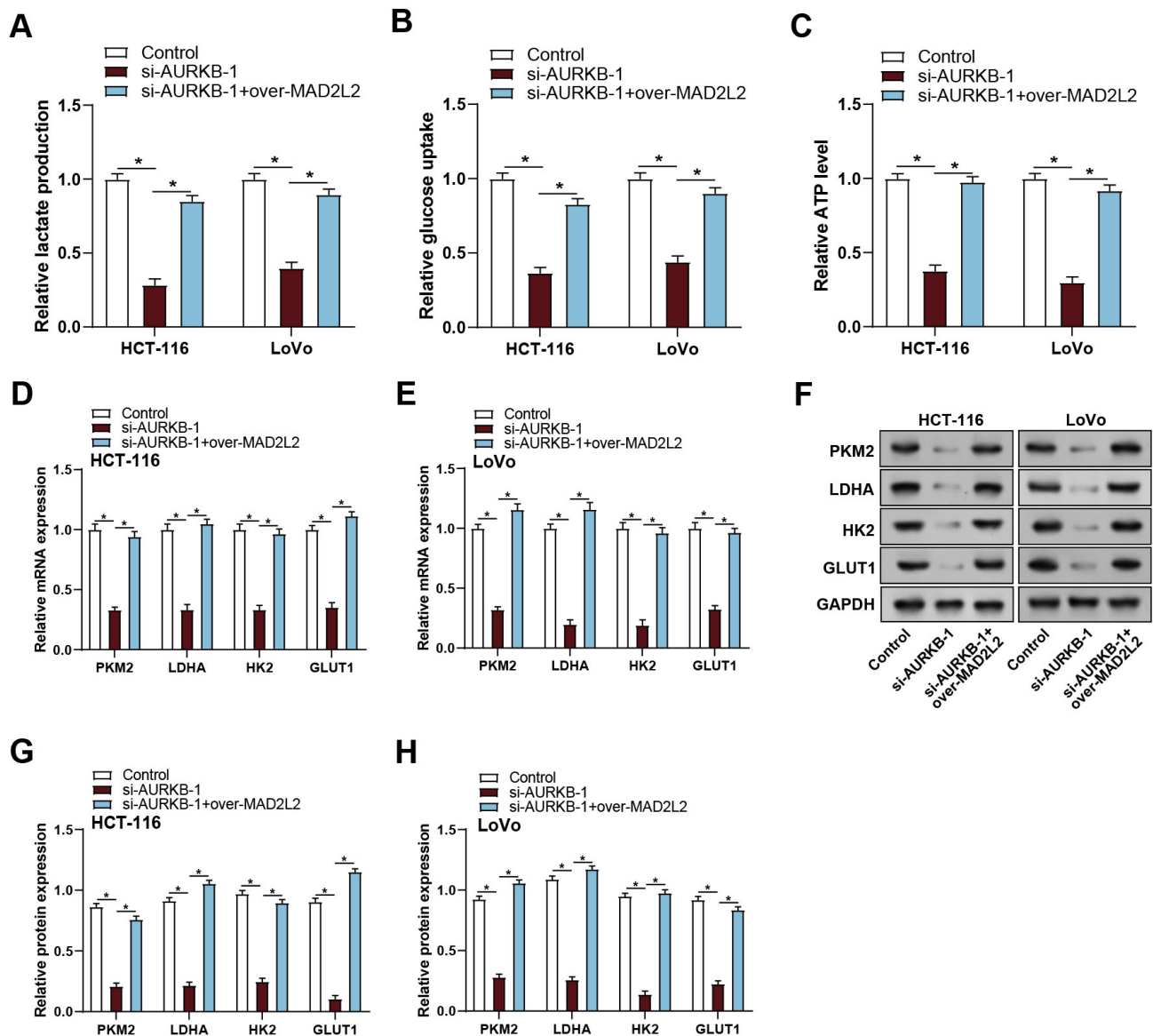


Fig. 11. Effects of *MAD2L2* overexpression on glycolysis and ATP production in *AURKB* knockdown CRC cells. (A) Lactate production levels in control, si-*AURKB*-1, si-*AURKB*-1+over-*MAD2L2* treated HCT-116 and LoVo cells. (B) Glucose uptake levels in control, si-*AURKB*-1, si-*AURKB*-1+over-*MAD2L2* treated HCT-116 and LoVo cells. (C) ATP levels in control, si-*AURKB*-1, si-*AURKB*-1+over-*MAD2L2* treated HCT-116 and LoVo cells. (D,E) qPCR was used to detect the mRNA expression levels of glycolysis-related genes *PKM2*, *LDHA*, *HK2*, and *GLUT1* in the control group, si-*AURKB*-1, si-*AURKB*-1+over-*MAD2L2* treated HCT-116 and LoVo cells. (F–H) Western blot analysis was used to detect the protein expression levels of glycolysis-related proteins *PKM2*, *LDHA*, *HK2*, and *GLUT1* in the control group, si-*AURKB*-1, si-*AURKB*-1+over-*MAD2L2* treated HCT-116 and LoVo cells. * $p < 0.05$. qPCR, quantitative PCR; *AURKB*, aurora kinase B; *MAD2L2*, mitotic arrest deficient 2 like 2; *PKM2*, pyruvate kinase M2; *LDHA*, lactate dehydrogenase, *HK2*, hexokinase 2; *GLUT1*, glucose transporter 1.

cose absorption are the hallmarks of this metabolic change, contributing to an acidic tumor microenvironment that promotes invasion and immune evasion in CRC cells [39]. Elevated ATP levels support the invasive behavior of these cells [40], and overexpression of glycolysis-related genes such as *HK2* and *GLUT1* enhances glucose metabolism in CRC [41,42]. We explored the impact of *AURKB* knockdown on oxidative stress and glycolysis in CRC cells. Our

results revealed that *AURKB* knockdown disrupted cellular oxidative balance and inhibited aerobic glycolysis, demonstrating that *AURKB* is essential for maintaining oxidative stress and glycolytic pathways in CRC cells. Therefore, targeting *AURKB* could impair the metabolism and viability of CRC cells by disrupting their oxidative stress response and glycolytic activity.

The DDR is critical for maintaining genomic stability by detecting and repairing DNA damage. Dysregulation of the DDR pathway in CRC leads to uncontrolled cell proliferation and tumorigenesis [43]. Defects in DDR mechanisms result in the accumulation of mutations, driving CRC progression and resistance to therapy [44]. Similarly, p53, a critical tumor suppressor involved in DDR, is often mutated in CRC, leading to impaired cell cycle control and resistance to apoptosis [25]. These disruptions in DDR promote genomic instability and contribute to the aggressive behavior of CRC cells. *MAD2L2*, a mitotic spindle assembly checkpoint component, is essential for cell cycle regulation and proper chromosome segregation. Dysregulation of *MAD2L2* has been noted in various cancers, such as CRC [45]. In CRC, *MAD2L2* overexpression is linked to poor prognosis and enhanced tumor invasiveness. According to a study, high levels of *MAD2L2* are related to increased proliferation, resistance to apoptosis, and the promotion of metastasis, underscoring its role in enhancing the invasive and migratory capabilities of CRC cells [46]. Our study further revealed a direct functional interaction between *AURKB* and *MAD2L2* in CRC progression, which provides a basis for understanding their synergistic effects. In addition, after *AURKB* knockdown, we observed a significant decrease in the expression *MAD2L2*, and the overexpression of *MAD2L2* did not restore the reduction in *AURKB* mRNA and protein expression caused by *AURKB* knockdown, suggesting that *AURKB* may positively regulate the expression of *MAD2L2*. This regulatory relationship suggests that *AURKB* may be critical in maintaining *MAD2L2* function. Moreover, overexpression of *MAD2L2* partially reversed the effects of *AURKB* knockdown on CRC cells, restoring cell proliferation, migration, and invasion abilities and attenuating the effects of cell cycle arrest and the DDR. These findings suggest that *MAD2L2* may play a compensatory role in maintaining cell metabolism and cell cycle progression after *AURKB* knockdown. Finally, *AURKB* and *MAD2L2* jointly regulate the p53 DDR pathway and aerobic glycolysis, critical pathways for CRC progression. The effects of *AURKB* knockdown and *MAD2L2* overexpression on these pathways suggest that they may synergistically regulate metabolism and DNA repair mechanisms in CRC cells. The findings of this study underscore the pivotal role of the *AURKB-MAD2L2* axis in modulating p53 DDR and metabolic pathways, highlighting its potential as a therapeutic target of CRC.

In this study, we revealed the potential role of *AURKB* and *MAD2L2* in CRC progression by *in vitro* experiments. However, we must recognize certain limitations in translating the results from *in vitro* experiments to clinical applications. First, *in vitro*, experimental conditions cannot fully mimic the complex tumor microenvironment in the human body. Factors such as tumor-host immune system interactions, tumor heterogeneity, and dynamic changes during tumor development are difficult to adequately capture in *in*

vitro models. These factors may impact the expression and function of *AURKB* and *MAD2L2*, thus limiting the generalizability of our results. Second, *in vitro* experiments usually cannot assess long-term therapeutic and side effects, which are very important considerations in clinical applications. Assessing these factors in an *in vivo* model is essential to determine the feasibility of *AURKB* and *MAD2L2* as therapeutic targets. In addition, there are significant individual differences and tumor heterogeneity among CRC patients, which may affect the expression and function of *AURKB* and *MAD2L2*. Our *in vitro* study failed to fully capture this heterogeneity, which may limit the generalizability of our results. Furthermore, CRC frequently develops resistance to therapy, and *in vitro* experiments may not be able to model this complex biological phenomenon fully. Therefore, investigating the roles of *AURKB* and *MAD2L2* in treatment resistance in an *in vivo* model is essential for developing effective therapeutic strategies. To overcome these limitations, we plan to incorporate *in vivo* models in future studies to validate the roles of *AURKB* and *MAD2L2* in CRC progression and to assess the *in vivo* effects of potential therapeutic strategies. We believe that with these additional studies, we can provide a stronger scientific foundation for *AURKB* and *MAD2L2* as therapeutic targets for CRC.

5. Conclusion

In conclusion, the research revealed that *AURKB* is a critical regulator of CRC cell proliferation, invasion, oxidative stress, and glycolysis. Our findings demonstrated that *AURKB* knockdown significantly inhibited CRC cell growth and metastasis while inducing apoptosis and disrupting the balance of oxidative stress and glycolysis. Furthermore, we discovered a novel interaction between *AURKB* and *MAD2L2*, elucidating their combined role in modulating the p53 DDR pathway and promoting aerobic glycolysis. These results suggest that targeting the *AURKB-MAD2L2* axis could be a promising therapeutic strategy for CRC. Our study provides new insights into the molecular underpinnings of CRC while discovering potential targets for future cancer research and treatment.

Declaration of AI and AI-assisted Technologies in the Writing Process

While preparing this research, the authors used artificial intelligence technology, ChatGPT, to assist in proofreading spelling and grammar. This tool was focused on the initial draft stage of the manuscript to help us identify and correct spelling and grammatical errors in the text. After initial language editing using ChatGPT, the authorsthoroughly reviewed the manuscript content and edited it as necessary to ensure scientific accuracy, clarity of expression, and originality of the article. We solemnly declare that the authors take full responsibility for the content of the final submitted publication despite using artificial intel-

ligence aids. We ensure that all opinions, data, and conclusions in the manuscript are derived from our research and analysis and do not infringe copyright or intellectual property rights.

Availability of Data and Materials

The datasets used and/or analyzed during the current study are available from the corresponding author upon reasonable request.

Author Contributions

Conception and design of the research: BS, SL, ZY and JX. Acquisition of data: SL. Analysis and interpretation of data: SL, JY, KY, CX, ZQ, YX, LY, and TZ. Statistical analysis: JY, KY, CX, ZQ, YX, LY, and TZ. Drafting the manuscript: SL and ZY. Revision of manuscript for important intellectual content: BS and JX. All authors contributed to editorial changes in the manuscript. All authors read and approved the final manuscript. All authors have participated sufficiently in the work and agreed to be accountable for all aspects of the work.

Ethics Approval and Consent to Participate

Not applicable.

Acknowledgment

Not applicable.

Funding

This research received no external funding.

Conflict of Interest

The authors declare no conflict of interest.

Supplementary Material

Supplementary material associated with this article can be found, in the online version, at <https://doi.org/10.31083/FBL26532>.

References

- [1] Xi Y, Xu P. Global colorectal cancer burden in 2020 and projections to 2040. *Translational Oncology*. 2021; 14: 101174. <https://doi.org/10.1016/j.tranon.2021.101174>.
- [2] Bray F, Laversanne M, Sung H, Ferlay J, Siegel RL, Soerjomataram I, *et al*. Global cancer statistics 2022: GLOBOCAN estimates of incidence and mortality worldwide for 36 cancers in 185 countries. *CA: a Cancer Journal for Clinicians*. 2024; 74: 229–263. <https://doi.org/10.3322/caac.21834>.
- [3] Duan B, Zhao Y, Bai J, Wang J, Duan X, Luo X, *et al*. *Gastrointestinal Cancers*. Exon Publications: Brisbane, Australia. 2022.
- [4] Lee MW, Kim JS, Kim JY, Lee KH. Prognostic Factor and Survival Benefit of Adjuvant Chemotherapy in Stage IIA Colon Cancer. *Annals of Coloproctology*. 2021; 37: 35–43. <https://doi.org/10.3393/ac.2020.09.03>.
- [5] Faubert B, Solmonson A, DeBerardinis RJ. Metabolic reprogramming and cancer progression. *Science (New York, N.Y.)*. 2020; 368: eaaw5473. <https://doi.org/10.1126/science.aaw5473>.
- [6] Santos JM, Hussain F. Higher Glucose Enhances Breast Cancer Cell Aggressiveness. *Nutrition and Cancer*. 2020; 72: 734–746. <https://doi.org/10.1080/01635581.2019.1654527>.
- [7] Zhao Y, Li N, Zhao J, Shi S. High expression of hexokinase 2 promotes lung cancer proliferation and metastasis. *Archives of Medical Science*. 2020; 8: 56081–56094.
- [8] Zhu Q, Ding L, Zi Z, Gao S, Wang C, Wang Y, *et al*. Viral-Mediated AURKB Cleavage Promotes Cell Segregation and Tumorigenesis. *Cell Reports*. 2019; 26: 3657–3671.e5. <https://doi.org/10.1016/j.celrep.2019.02.106>.
- [9] Varshney N, Rani A, Kashyap D, Tiwari D, Jha HC. Aurora kinase: An emerging potential target in therapeutics. *Protein Kinase Inhibitors* (pp. 261–322). Elsevier: Amsterdam, Netherlands. 2022.
- [10] Shah ET, Molloy C, Gough M, Kryza T, Samuel SG, Tucker A, *et al*. Inhibition of Aurora B kinase (AURKB) enhances the effectiveness of 5-fluorouracil chemotherapy against colorectal cancer cells. *British Journal of Cancer*. 2024; 130: 1196–1205. <https://doi.org/10.1038/s41416-024-02584-z>.
- [11] Hicks HM, Nassar VL, Lund J, Rose MM, Schweppe RE. The effects of Aurora Kinase inhibition on thyroid cancer growth and sensitivity to MAPK-directed therapies. *Cancer Biology & Therapy*. 2024; 25: 2332000. <https://doi.org/10.1080/15384047.2024.2332000>.
- [12] Marima R, Hull R, Penny C, Dlamini Z. Mitotic syndicates Aurora Kinase B (AURKB) and mitotic arrest deficient 2 like 2 (MAD2L2) in cohorts of DNA damage response (DDR) and tumorigenesis. *Mutation Research. Reviews in Mutation Research*. 2021; 787: 108376. <https://doi.org/10.1016/j.mrrev.2021.108376>.
- [13] Liu Z, Wang S, Yu K, Chen K, Zhao L, Zhang J, *et al*. The promoting effect and mechanism of MAD2L2 on stemness maintenance and malignant progression in glioma. *Journal of Translational Medicine*. 2023; 21: 863. <https://doi.org/10.1186/s12967-023-04740-0>.
- [14] Bosshard S, Duroy PO, Mermoud N. A role for alternative end-joining factors in homologous recombination and genome editing in Chinese hamster ovary cells. *DNA Repair*. 2019; 82: 102691. <https://doi.org/10.1016/j.dnarep.2019.102691>.
- [15] Li L, Jiang P, Hu W, Zou F, Li M, Rao T, *et al*. AURKB promotes bladder cancer progression by deregulating the p53 DNA damage response pathway via MAD2L2. *Journal of Translational Medicine*. 2024; 22: 295. <https://doi.org/10.1186/s12967-024-05099-6>.
- [16] Jin W, Zhang J, Chen X, Yin S, Yu H, Gao F, *et al*. Unraveling the complexity of histone-arginine methyltransferase CARM1 in cancer: From underlying mechanisms to targeted therapeutics. *Biochimica et Biophysica Acta. Reviews on Cancer*. 2023; 1878: 188916. <https://doi.org/10.1016/j.bbcan.2023.188916>.
- [17] Kim JJ, Lee SY, Miller KM. Preserving genome integrity and function: the DNA damage response and histone modifications. *Critical Reviews in Biochemistry and Molecular Biology*. 2019; 54: 208–241. <https://doi.org/10.1080/10409238.2019.1620676>.
- [18] Catalano F, Borea R, Puglisi S, Boutros A, Gandini A, Cremonese M, *et al*. Targeting the DNA Damage Response Pathway as a Novel Therapeutic Strategy in Colorectal Cancer. *Cancers*. 2022; 14: 1388. <https://doi.org/10.3390/cancers14061388>.
- [19] Liu R, Zhang Q, Shen L, Chen S, He J, Wang D, *et al*. Long noncoding RNA Inc-RI regulates DNA damage repair and radiation sensitivity of CRC cells through NHEJ pathway. *Cell Biology and Toxicology*. 2020; 36: 493–507. <https://doi.org/10.1007/s10565-020-09524-6>.
- [20] Deng S, Vlatkovic T, Li M, Zhan T, Veldwijk MR, Herskind C. Targeting the DNA Damage Response and DNA Repair Path-

- ways to Enhance Radiosensitivity in Colorectal Cancer. *Cancers*. 2022; 14: 4874. <https://doi.org/10.3390/cancers14194874>.
- [21] Pilié PG, Gay CM, Byers LA, O'Connor MJ, Yap TA. PARP Inhibitors: Extending Benefit Beyond *BRCA*-Mutant Cancers. *Clinical Cancer Research: an Official Journal of the American Association for Cancer Research*. 2019; 25: 3759–3771. <https://doi.org/10.1158/1078-0432.CCR-18-0968>.
 - [22] Koch DT, Yu H, Beirith I, Schirren M, Drefs M, Liu Y, *et al.* Tigecycline causes loss of cell viability mediated by mitochondrial OXPHOS and RAC1 in hepatocellular carcinoma cells. *Journal of Translational Medicine*. 2023; 21: 876. <https://doi.org/10.1186/s12967-023-04615-4>.
 - [23] Cucchi D, Gibson A, Martin SA. The emerging relationship between metabolism and DNA repair. *Cell Cycle (Georgetown, Tex.)*. 2021; 20: 943–959. <https://doi.org/10.1080/15384101.2021.1912889>.
 - [24] Aitchison A, Hakkaart C, Day RC, Morrin HR, Frizelle FA, Keenan JL. *APC* Mutations Are Not Confined to Hotspot Regions in Early-Onset Colorectal Cancer. *Cancers*. 2020; 12: 3829. <https://doi.org/10.3390/cancers12123829>.
 - [25] Michel M, Kaps L, Maderer A, Galle PR, Moehler M. The Role of p53 Dysfunction in Colorectal Cancer and Its Implication for Therapy. *Cancers*. 2021; 13: 2296. <https://doi.org/10.3390/cancers13102296>.
 - [26] Meng M, Zhong K, Jiang T, Liu Z, Kwan HY, Su T. The current understanding on the impact of KRAS on colorectal cancer. *Biomedicine & Pharmacotherapy = Biomedecine & Pharmacotherapie*. 2021; 140: 111717. <https://doi.org/10.1016/j.biopha.2021.111717>.
 - [27] Shi C, Tao S, Ren G, Yang EJ, Shu X, Mou PK, *et al.* Aurora kinase A inhibition induces synthetic lethality in SMAD4-deficient colorectal cancer cells via spindle assembly checkpoint activation. *Oncogene*. 2022; 41: 2734–2748. <https://doi.org/10.1038/s41388-022-02293-y>.
 - [28] Gan Y, Li Y, Li T, Shu G, Yin G. CCNA2 acts as a novel biomarker in regulating the growth and apoptosis of colorectal cancer. *Cancer Management and Research*. 2018; 10: 5113–5124. <https://doi.org/10.2147/CMAR.S176833>.
 - [29] Bonetti D, Colombo CV, Clerici M, Longhese MP. Processing of DNA Ends in the Maintenance of Genome Stability. *Frontiers in Genetics*. 2018; 9: 390. <https://doi.org/10.3389/fgene.2018.00390>.
 - [30] Uusküla-Reimand L, Wilson MD. Untangling the roles of TOP2A and TOP2B in transcription and cancer. *Science Advances*. 2022; 8: eadd4920. <https://doi.org/10.1126/sciadv.add4920>.
 - [31] Zhang J, Ma J, Li Y, An Y, Du W, Yang Q, *et al.* Overexpression of Aurora Kinase B Is Correlated with Diagnosis and Poor Prognosis in Hepatocellular Carcinoma. *International Journal of Molecular Sciences*. 2024; 25: 2199. <https://doi.org/10.3390/ijms25042199>.
 - [32] Huang D, Huang Y, Huang Z, Weng J, Zhang S, Gu W. Relation of *AURKB* over-expression to low survival rate in BCRA and reversine-modulated aurora B kinase in breast cancer cell lines. *Cancer Cell International*. 2019; 19: 166. <https://doi.org/10.1186/s12935-019-0885-z>.
 - [33] Kaarijärvi R, Kaljunen H, Ketola K. Molecular and Functional Links between Neurodevelopmental Processes and Treatment-Induced Neuroendocrine Plasticity in Prostate Cancer Progression. *Cancers*. 2021; 13: 692. <https://doi.org/10.3390/cancer13040692>.
 - [34] Shen L, Qu X, Li H, Xu C, Wei M, Wang Q, *et al.* NDRG2 facilitates colorectal cancer differentiation through the regulation of Skp2-p21/p27 axis. *Oncogene*. 2018; 37: 1759–1774. <https://doi.org/10.1038/s41388-017-0118-7>.
 - [35] Gu YY, Chen MH, May BH, Liao XZ, Liu JH, Tao LT, *et al.* Matrine induces apoptosis in multiple colorectal cancer cell lines in vitro and inhibits tumour growth with minimum side effects in vivo via Bcl-2 and caspase-3. *Phytomedicine: International Journal of Phytotherapy and Phytopharmacology*. 2018; 51: 214–225. <https://doi.org/10.1016/j.phymed.2018.10.004>.
 - [36] Afzal S, Abdul Manap AS, Attiq A, Albokhdaïm I, Kandeel M, Alhojaily SM. From imbalance to impairment: the central role of reactive oxygen species in oxidative stress-induced disorders and therapeutic exploration. *Frontiers in Pharmacology*. 2023; 14: 1269581. <https://doi.org/10.3389/fphar.2023.1269581>.
 - [37] Basak D, Uddin MN, Hancock J. The Role of Oxidative Stress and Its Counteractive Utility in Colorectal Cancer (CRC). *Cancers*. 2020; 12: 3336. <https://doi.org/10.3390/cancers12113336>.
 - [38] Fan T, Sun G, Sun X, Zhao L, Zhong R, Peng Y. Tumor Energy Metabolism and Potential of 3-Bromopyruvate as an Inhibitor of Aerobic Glycolysis: Implications in Tumor Treatment. *Cancers*. 2019; 11: 317. <https://doi.org/10.3390/cancers11030317>.
 - [39] Nicolini A, Ferrari P. Involvement of tumor immune microenvironment metabolic reprogramming in colorectal cancer progression, immune escape, and response to immunotherapy. *Frontiers in Immunology*. 2024; 15: 1353787. <https://doi.org/10.3389/fimmu.2024.1353787>.
 - [40] Lin CS, Liu LT, Ou LH, Pan SC, Lin CI, Wei YH. Role of mitochondrial function in the invasiveness of human colon cancer cells. *Oncology Reports*. 2018; 39: 316–330. <https://doi.org/10.3892/or.2017.6087>.
 - [41] Dai W, Meng X, Mo S, Xiang W, Xu Y, Zhang L, *et al.* FOXE1 represses cell proliferation and Warburg effect by inhibiting HK2 in colorectal cancer. *Cell Communication and Signaling: CCS*. 2020; 18: 7. <https://doi.org/10.1186/s12964-019-0502-8>.
 - [42] Li C, Chen Q, Zhou Y, Niu Y, Wang X, Li X, *et al.* S100A2 promotes glycolysis and proliferation via GLUT1 regulation in colorectal cancer. *FASEB Journal: Official Publication of the Federation of American Societies for Experimental Biology*. 2020; 34: 13333–13344. <https://doi.org/10.1096/fj.202000555R>.
 - [43] Rivas-Domínguez A, Pastor N, Martínez-López L, Colón-Pérez J, Bermúdez B, Orta ML. The Role of DNA Damage Response in Dysbiosis-Induced Colorectal Cancer. *Cells*. 2021; 10: 1934. <https://doi.org/10.3390/cells10081934>.
 - [44] Tomasini PP, Guecheva TN, Leguisamo NM, Péricart S, Brunac AC, Hoffmann JS, *et al.* Analyzing the Opportunities to Target DNA Double-Strand Breaks Repair and Replicative Stress Responses to Improve Therapeutic Index of Colorectal Cancer. *Cancers*. 2021; 13: 3130. <https://doi.org/10.3390/cancer13133130>.
 - [45] Li Y, Li L, Chen M, Yu X, Gu Z, Qiu H, *et al.* MAD2L2 inhibits colorectal cancer growth by promoting NCOA3 ubiquitination and degradation. *Molecular Oncology*. 2018; 12: 391–405. <https://doi.org/10.1002/1878-0261.12173>.
 - [46] Sun H, Wang H, Li X, Hao Y, Ling J, Wang H, *et al.* Increased MAD2L2 expression predicts poor clinical outcome in Colon Adenocarcinoma. *Biocell*. 2023; 47: 607–618.